QUAS-R: An SLC1A5-mediated glutamine uptake assay with single-cell resolution reveals metabolic heterogeneity with immune populations

Pelgrom, L.R.; Davis, G.M.; O'Shaughnessy, S.; Wezenberg, E.J.M.; Kasteren, S.I. van; Finlay, D.K.; Sinclair, L.V.

Cell Reports

Article

QUAS-R: An SLC1A5-mediated glutamine uptake assay with single-cell resolution reveals metabolic heterogeneity with immune populations

Graphical abstract

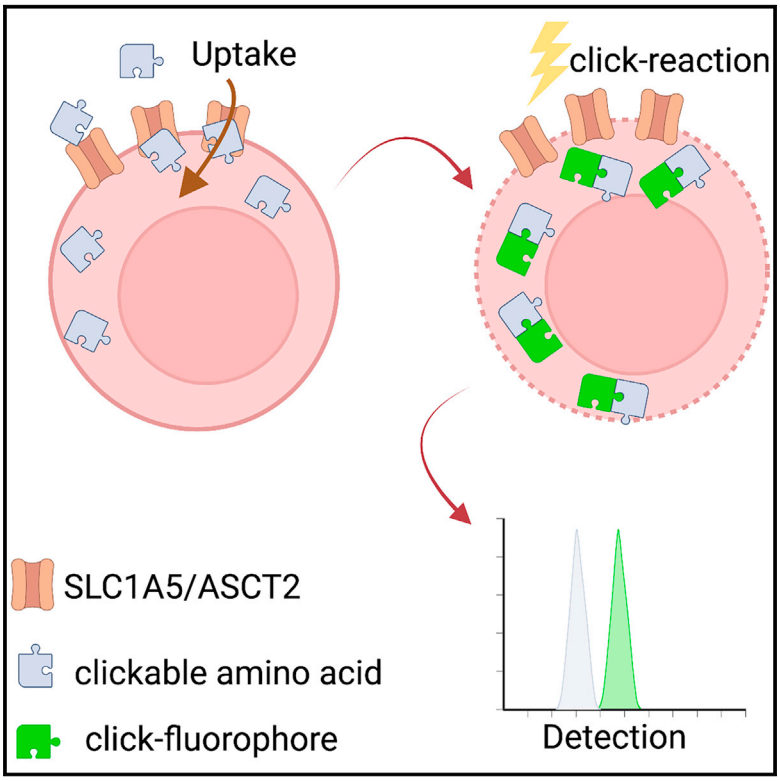

Highlights

- Bioorthogonal amino acids AHA and HPG are transported by SLC1A5, a key glutamine transporter
- Click chemistry-targeted fluorophores report SLC1A5 transport with single-cell resolution
- HPG uptake *in vivo* by immune cells, visualized by *ex vivo* fluorophore conjugation
- An assay to report glutamine uptake of individual cells in complex immune microenvironments

Authors

Leonard R. Pelgrom, Gavin M. Davis, Simon O'Shaughnessy, Emilie J.M. Wezenberg, Sander I. Van Kasteren, David K. Finlay, Linda V. Sinclair

Correspondence

s.i.van.kasteren@chem.leidenuniv.nl (S.I.V.K.), finlayd@tcd.ie (D.K.F.), l.v.sinclair@dundee.ac.uk (L.V.S.)

In brief

Pelgrom et al. describe a method with which to monitor glutamine uptake at a single-cell level. This assay reveals and unlocks the cellular heterogeneity in glutamine metabolism that is currently unreachable. This is a significant advancement for the field, allowing accurate studies of nutrient uptake in complex microenvironments.

Pelgrom et al., 2023, Cell Reports *42*, 112828
August 29, 2023
https://doi.org/10.1016/j.celrep.2023.112828

CellPress

Cell Reports

CellPress
OPEN ACCESS

Article

QUAS-R: An SLC1A5-mediated glutamine uptake assay with single-cell resolution reveals metabolic heterogeneity with immune populations

Leonard R. Pelgrom,[1,5] Gavin M. Davis,[2,5] Simon O'Shaughnessy,[2] Emilie J.M. Wezenberg,[1] Sander I. Van Kasteren,[1,6,*] David K. Finlay,[2,3,6,*] and Linda V. Sinclair[4,6,7,*]

[1]Leiden Institute of Chemistry and the Institute of Chemical Immunology, Leiden University, Einsteinweg 55, 2333 CC Leiden, the Netherlands
[2]School of Biochemistry and Immunology, Trinity Biomedical Sciences Institute, Trinity College Dublin, 152-160 Pearse Street, D02R590 Dublin, Ireland
[3]School of Pharmacy and Pharmaceutical Sciences, Trinity Biomedical Sciences Institute, Trinity College Dublin, 152-160 Pearse Street, D02R590 Dublin, Ireland
[4]School of Life Sciences, University of Dundee, Dow Street, Dundee DD1 5EH, Scotland, UK
[5]These authors contributed equally
[6]Senior author
[7]Lead contact
*Correspondence: s.i.van.kasteren@chem.leidenuniv.nl (S.I.V.K.), finlayd@tcd.ie (D.K.F.), l.v.sinclair@dundee.ac.uk (L.V.S.)
https://doi.org/10.1016/j.celrep.2023.112828

SUMMARY

System-level analysis of single-cell data is rapidly transforming the field of immunometabolism. Given the competitive demand for nutrients in immune microenvironments, there is a need to understand how and when immune cells access these nutrients. Here, we describe a new approach for single-cell analysis of nutrient uptake where we use in-cell biorthogonal labeling of a functionalized amino acid after transport into the cell. In this manner, the *bona fide* active uptake of glutamine via SLC1A5/ASCT2 could be quantified. We used this assay to interrogate the transport capacity of complex immune subpopulations, both *in vitro* and *in vivo*. Taken together, our findings provide an easy sensitive single-cell assay to assess which cells support their function via SLC1A5-mediated uptake. This is a significant addition to the single-cell metabolic toolbox required to decode the metabolic landscape of complex immune microenvironments.

INTRODUCTION

Immune cells have a highly dynamic physiology whereby their metabolic and biosynthetic capacities are dramatically regulated in response to immune stimulation.[1] Immune activated T cells, for example, clonally expand and differentiate into effector cells capable of producing cytokines and/or cytolytic molecules that help to clear pathogen-infected or tumor cells. These critical functions of diverse immune cells must be fueled, both in energetic terms as well as through the provision of raw building materials.

The metabolic processes that underpin these dynamic changes in immune cell activity and function have become a focus of research since it became clear that metabolic interventions can have real therapeutic benefits.[2,3] Modulating immune cell metabolism has the potential to support beneficial immune function, prevent dysfunctional responses, or even restore correct immune function in pathological settings. For example, inhibition of glutamine metabolism within the tumor microenvironment has been shown to benefit antitumor CD8 T cell responses.[4] One issue that hampers the development of new metabolism-targeting treatments is that metabolic measurements on whole populations of immune cells cultured *in vitro* do not accurately reflect immune cell metabolism, as it occurs *in vivo*. Therefore, we need technologies to measure cellular metabolism at single-cell resolution either *in vivo* or directly *ex vivo*. The lack of such technologies represents a major barrier to understanding the actual immunometabolic processes occurring in complex immune populations *in vivo*.

Protein synthesis is a highly energy-dependent process reliant on the supply of ATP and amino acids and is finely balanced with concurrent cellular protein degradation processes. Cellular uptake of nutrients is essential for the elevated protein synthesis associated with dynamic immune responses; this uptake provides catabolites for energy production and anabolites used for protein synthesis and proliferation. In the context of T cell activation, multiple high-resolution proteomics studies have demonstrated that naive T cells have low levels of nutrient transporter expression and correspondingly low levels of nutrient uptake.[5–7] A critical early feature of T cell activation is the coordinated increase in the expression of multiple nutrient transporters, including amino acid transporters SLC7A5 (also called L-type amino acid transporter 1; LAT1) and SLC1A5 (also called alanine, serine, cysteine transporter 2; ASCT2).[8,9] Indeed, we

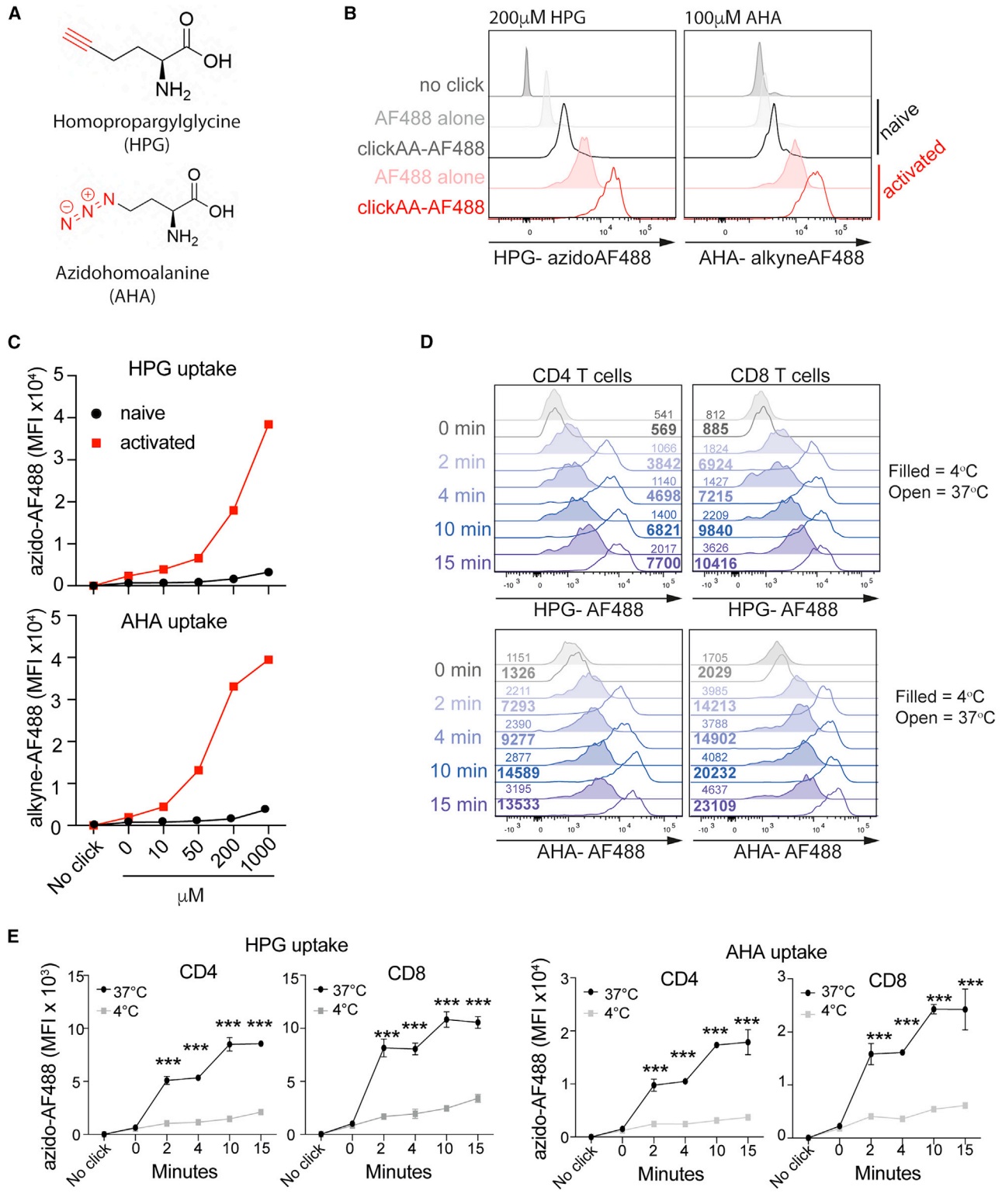

Figure 1. Activated T cells take up bioorthogonal amino acids

(A) Bioorthogonal amino acids homopropargylglycine (HPG) and azidohomoalanine (AHA).

(B) HPG (200 μM) or AHA (100 μM) was provided to *ex vivo* (naive) or activated (anti-CD3/CD28; 24 h) T cells for 15 min prior to fixation and subsequent copper-click reaction with alkyne-AF488 or azide-AF488. No click reaction (HPG or AHA alone) or fluorophore-alone controls are shown.

(legend continued on next page)

know that limiting amounts of key nutrients including glucose, methionine, arginine, and glutamine alter and dampen the T cell effector responses.[6,9–12]

Therefore, measuring and quantifying nutrient uptake at a single-cell resolution directly *ex vivo* would provide valuable insight into immunometabolic activity or potential, thereby generating the high-resolution data required to resolve metabolic heterogeneity within complex immune environments. To date, this has been largely unachievable because conventional nutrient uptake assays involve tracking uptake of radiolabeled substrates into cells, which is not compatible with single-cell approaches such as flow cytometry and microscopy. One approach has been the use of fluorophore-labeled nutrient analogs as markers for transporter activity, such as bodipy-labeled lipids or 7-nitrobenzofurazan-labeled glucose (NBDG). However, attaching a fluorophore to a nutrient will, in most cases, dramatically change the transport characteristics of that nutrient, and so this approach is largely inaccurate. For instance, fluorophore-modified lipids accumulate in different compartments than lipids modified with smaller detectable groups,[13] and fluorescently tagged glucose (2-deoxy-2-[(7-nitro-2,1,3-benzoxadiazol-4-yl) amino]-D-glucose [2NBDG]) is not transported by the glucose transporters expressed on immune cells, SLC2A1 and SLC2A3.[14–16] For amino acids, various fluorescent analogs have been synthesized. However, the transporter specificity of these have not been ascertained. The only well-characterized fluorescent reagent for measuring transporter activity has been the naturally fluorescent kynurenine. This tryptophan metabolite provides a convenient method to measure activity of the system L amino acid transporter SLC7A5.[17] However, for most transporters, a convenient fluorescent cargo has not been identified.

One approach that has been gaining traction in carbohydrate and lipid studies has been the use of bioorthogonal reagents in combination with cell-compatible click chemistry.[18–20] In BONCAT (bioorthogonal non-canonical amino acid tagging), a metabolite is modified with a functional chemical group that is both small and stable within the conditions found in a cell.[21] Then, at the end of a labeling period, this metabolite is visualized within the cell by the highly selective ligation of a fluorophore (or other detection mode) that is itself modified with a chemical group that can selectively react with the chemical group that was introduced in the metabolite. This approach has been extensively used to label many cellular components, such as glycans,[21,22] lipids,[23,24] DNA[25] and RNA[26] from bacteria,[27] cell lines, and even whole animals, such as zebrafish and mice.[28,29] In 2002, it was reported that amino acids carrying such bioorthogonal groups (in this case, azidohomoalanine) could be incorporated into the *E. coli* proteome in place of methionine and be used to ligate a protein with a Staudinger ligation reaction,[30] and later, the alkyne-containing homopropargylglycine was used and ligated via a copper-catalyzed Huisgen azide-alkyne cycloaddition (CCAAC) reaction.[31] In 2006, Tirrell and co-workers reported the use of this same approach to label methionine throughout the entire proteome of a mammalian cell line.[32] This approach has since been applied to the study of protein synthesis in many species.[33] Yet, despite the broad application of the BONCAT approach, the transporter specificity of these two "functionalized" amino acids has never been specified. Whether they are transported by the same route as the unmodified methionine is unknown.

Herein, we investigated whether certain bioorthogonal amino acids can be used to achieve rapid, sensitive uptake measurements for a defined amino acid transporter with single-cell resolution. We characterize the uptake of the bioorthogonally reactive amino acids azidohomoalanine (AHA) and homopropargylglycine (HPG) and—to our surprise—find it to be through SLC1A5/ASCT2, the major glutamine transporter expressed in immune cells. We then demonstrate that this bioorthogonal amino acid uptake approach delivers an accurate and quantitative single-cell measure of SLC1A5-mediated amino acid uptake capacity. Furthermore, we validate the ability of this assay to resolve metabolically distinct cells in a complex, multipopulation immune scenario through studying the SLC1A5-mediated amino acid uptake capacity of developing T cells in the thymus and of immune populations in the spleen.

RESULTS

Activated T cells take up bioorthogonal amino acids

It is well established that bioorthogonal amino acids can also be taken up by mammalian cells *in vitro*. For instance, AHA and HPG have been shown to be taken up by mammalian cells and incorporated into proteins at the positions of methionine.[32,34] HPG contains an alkyne functional group, whereas AHA contains an azide functional group (Figure 1A). However, the transporters that mediate cellular uptake of these bioorthogonal amino acids are unknown. We first confirmed that immune activated T cells take up bioorthogonal amino acids, HPG and AHA. Unstimulated or immune activated (anti-CD3/CD28) T cells were incubated with HPG or AHA for 15 min, followed by cell fixation and permeabilization. The abundance of HPG/AHA inside the cell was detected by ligating azido-AF488 or alkyne-AF488 to the HPG and AHA, respectively. Background fluorescence of azido-AF488 or alkyne-AF488 was determined by using T cells that were not provided with HPG or AHA but were treated equivalently thereafter (Figure 1B). Activated T cells take significantly more HPG or AHA than naive T cells (Figures 1B and 1C). There was also a difference in background staining with azido-AF488/alkyne-AF488 compounds between unstimulated and activated cells. This highlighted the importance of including these

(C) Uptakes performed as in (B) with increasing concentrations of HPG or AHA as indicated; data are presented as adjusted uptake MFI (total MFI − background MFI).

(D and E) Uptakes performed as in (B) using HPG (100 μM) or AHA (100 μM) but for intervals of 0–15 min and at either 4°C (filled histograms) or 37°C (open histograms). Data are shown separately for CD4 and CD8 T cells as representative histograms (D) and pooled adjusted MFI data (MFI − MFI from no click controls) from 3 biological replicates (E).

Data are representative of 3 independent experiments (B–D) or mean ± SD of 3 biological replicates (E). Data are analyzed using multiple unpaired t tests (E) (*$p < 0.05$; **$p < 0.01$; ***$p < 0.001$).

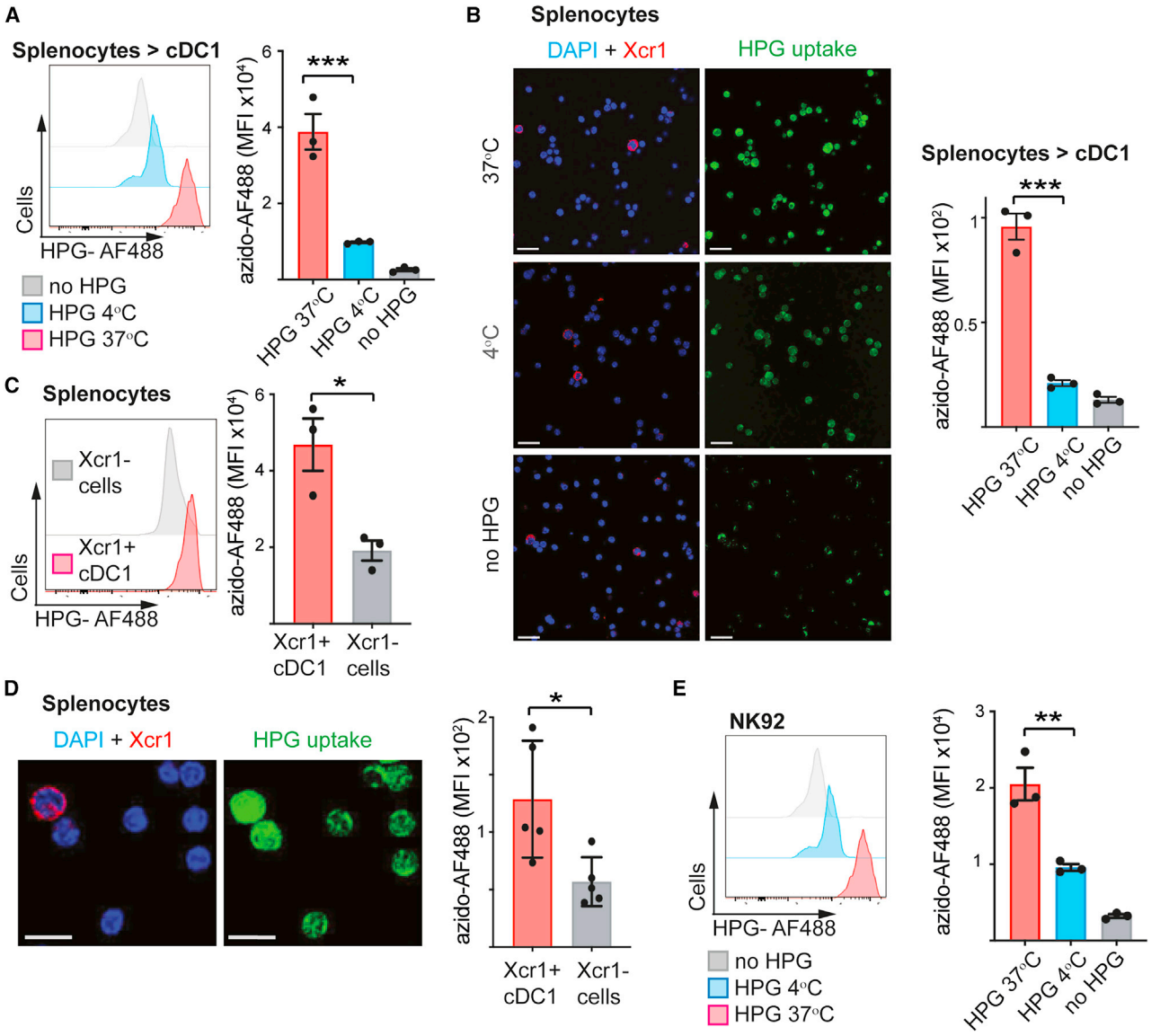

Figure 2. Type 1 dendritic cells and human NK cells take up bioorthogonal amino acids

(A) Splenocytes were stained with surface antibodies prior to 2 min uptake of HPG (200 μM) at either 37°C or 4°C, followed by fixation and copper-click addition of azide-AF488. Representative histogram (left) and pooled data (right) for major histocompatibility complex (MHC) class II^{high}, CD11c^{+} Xcr1^{+} cDC1s.

(B) Parallel microscopy images of splenocytes, as in (A), co-stained with nuclear stain DAPI (blue) and cDC1 marker Xcr1-AF647 (red), with corresponding images showing HPG-AF488 uptake in green. Scale bars: 20 μm. Quantification of pooled data is shown in the bar chart (right).

(C) HPG uptakes performed at 37°C, as in (A), gating on Xcr1^{-} and Xcr1^{+} splenocytes. Representative histogram (left) and pooled data (right).

(D) Confocal microscopy images, as in (B), showing Xcr1^{+} and Xcr1^{-} splenocytes (right) and quantification (right). Scale bars: 10 μm.

(E) HPG (200 μM) uptake into human NK92 cells, as in (A), showing a representative histogram (left) and pooled data (right).

Data are mean ± SEM or representative of 3 (A–C and E) and 5 (D) independent experiments. Data points in bar charts indicate biological replicates. Data are analyzed using a one-way ANOVA with a Dunnet's post-test (A, B, and E) or a Student's t test (C and D) (*p < 0.05; **p < 0.01; ***p < 0.001).

conditions in the assay and adjusting the mean fluorescence intensity (MFI) values to evaluate the uptake accordingly: uptake MFI = total MFI − background MFI (Figure 1C). Naive T cells show very low uptake, while there was a clear uptake of HPG and AHA in activated T cells when provided at concentrations greater than or equal to 10 μM (Figure 1B). Neither HPG nor AHA was toxic to T cells at any of the concentrations used (Figure S1). Next, the uptake was measured over time into activated CD4 and CD8 T cells at either 37°C or 4°C to determine kinetics of the bioorthogonal amino acid transport. Consistent with active transporter-mediated uptake, there was a rapid accumulation of biorthogonal amino acids in both activated CD4 and CD8 T cells within 2 min that was blocked when the assay was performed at 4°C (Figures 1D and 1E). Short incubation (2–3 min) times were

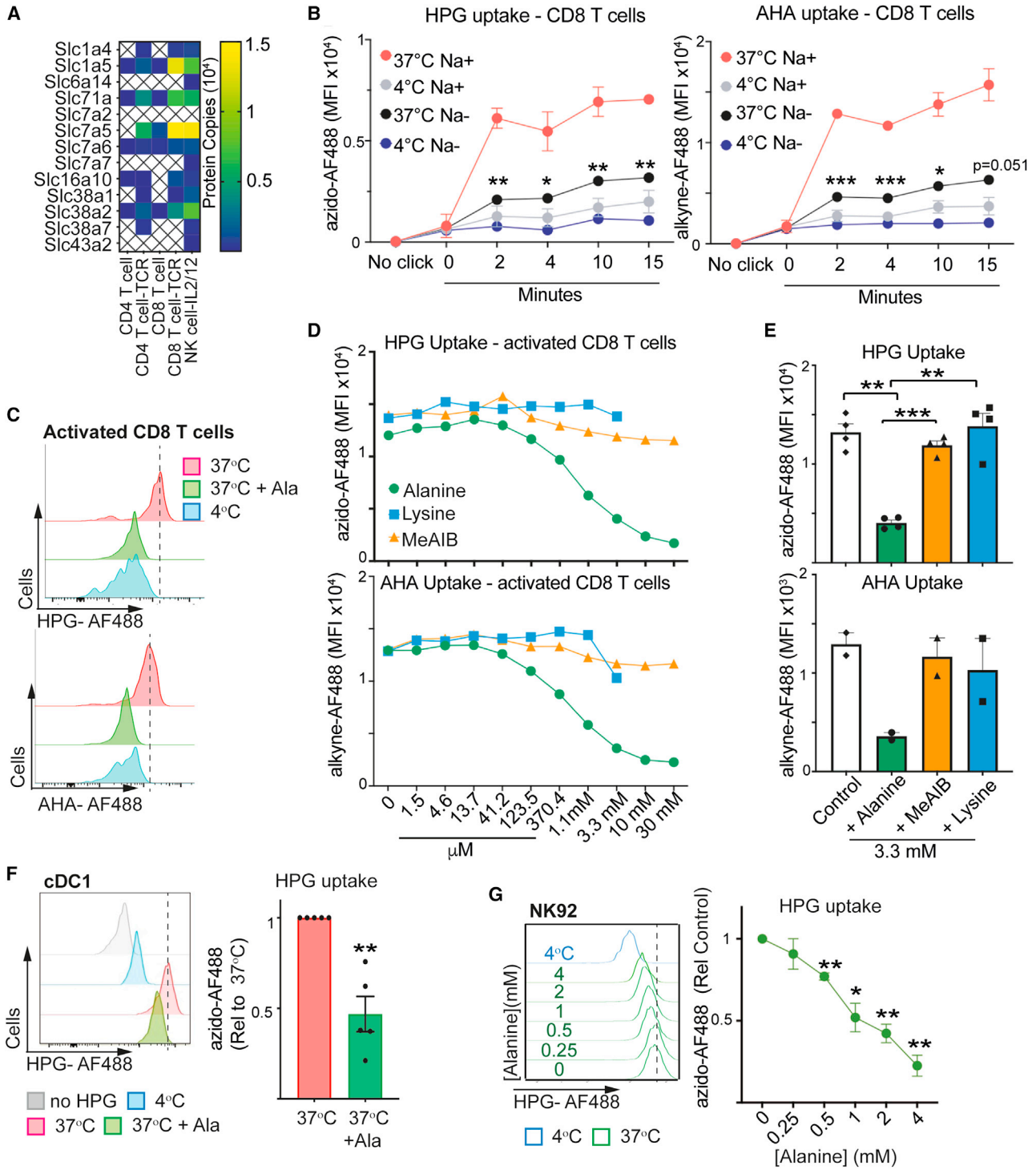

Figure 3. Identification of SLC1A5 as the transporter of HPG and AHA in immune cells

(A) Heatmap showing protein expression of amino acid transporters in murine naive and TCR activated CD4 T cells, naive and TCR activated CD8 T cells, and IL-2/-12 activated NK cells. Blue (low) to yellow (high) with corresponding protein copy numbers indicated. Data are from immpres.co.uk.[37,57]

(B) Activated (anti-CD3/CD28 treated; 24 h) CD8 T cells were provided HPG (100 μM) or AHA (100 μM) in Na^+-containing or Na-free media at 37°C or 4°C for indicated times. Data are background adjusted MFI values.

(C) 2 min HPG (400 μM, top panel) or AHA (100 μM; bottom panel) uptake into activated CD8 T cells ± alanine (5 mM). Uptake at 4°C also shown.

(legend continued on next page)

used as the basis for the standard uptake assay from here onward. We wanted to verify the efficiency of the fixation conditions regarding retention of the bioorthogonal amino acids within the cells. When activated T cells were fixed after 3 min of bioorthogonal amino acid uptake and then kept for up to 14 days at 4°C before permeabilization and subsequent click reaction and detection, no signal loss was observed (Figure S1B).

In separate experiments the uptake of HPG into type 1 dendritic cells (cDC1) was measured by both flow cytometry and confocal microscopy (Figures 2A and 2B). As a tool to expand DCs *in vivo*, C57Bl/6 mice were injected with Flt3-secreting B16 cells subcutaneously in the flank, and spleens were harvested after 8 days.[35,36] Splenocytes were stained with surface antibodies to identify cDC1^{Xcr1+} and then provided with HPG for 2 min at either 37°C or 4°C before fixation and permeabilization. Uptake of HPG was visualized as described above using azido-AF488 and the copper-click conjugation reaction. There was a significant HPG uptake signal detected by flow cytometry in cDC1s at 37°C that was prevented when the uptake was performed at 4°C (Figure 2A). In parallel, we performed uptake assays on *ex vivo* splenocytes allowed to settle on coverslips. The splenocytes were fixed and stained with Xcr1 and the copper-click conjugation with azido-AF488 to detect HPG uptake. Similar to the flow cytometry assay, HPG uptake in cDC1^{Xcr1+} splenocytes was inhibited at 4°C (Figure 2B). Furthermore, uptake of HPG into cDC1^{Xcr1+} was found to be significantly greater than that of non-cDC1 splenocytes (Xcr1^{-} cells) both by flow cytometry and confocal microscopy (Figures 2C and 2D).

While murine and human amino acid transporters share substantial protein homology, it was nevertheless important to test whether the bioorthogonal amino acid HPG is similarly transported into human immune cells. To investigate this, we used the human NK cell line, NK92, and measured a significant uptake signal when cells were provided HPG for 2 min at 37°C, and this signal was largely reduced when the uptake was performed at 4°C (Figure 2E).

HPG and AHA are transported by the glutamine transporter SLC1A5

Activated lymphocytes express multiple amino acid transporters (Figure 3A), and so experiments were designed to define which transporter is responsible for the uptake of HPG and AHA. Amino acid transporters can be identified based upon biochemical and biophysical transport parameters. For example, system L transporters are sodium independent, whereas substrate transport via system ASC and system N and A transporters (SNATs) are sodium dependent. As previously mentioned, the bioorthogonal amino acids AHA and HPG are incorporated into proteins in place of methionine, which means that they bind to the methionine-specific tRNA for use during protein translation.[32,34] If AHA and HPG are also transported similarly to methionine, they would be transported by the sodium-independent amino acid transporter SLC7A5, the primary methionine transporter in activated T cells.[6] It was, therefore, surprising that the uptake of HPG and AHA into CD8 T cells was sodium dependent (Figure 3B). Uptake was measured in sodium-containing and sodium-free buffers, and the data showed that uptake of both HPG and AHA was reduced to the level of the 4°C control in the sodium-free buffer (Figure 3B). Similar data were obtained with activated CD4 T cells (Figure S2A). This indicates that transport is not via SLC7A5 but is instead mediated via a sodium-dependent amino acid transporter. To further explore what transporter is required for AHA and HPG uptake, competition experiments were performed with amino acids known to be substrates for sodium-dependent transporters. It was found that uptake of both HPG and AHA was inhibited by competition with alanine (Figure 3C). Activated T cells increase the expression of two sodium-dependent alanine transporter families: SLC1 (SLC1A5) and SLC38 (SLC38A1 and A2) (Figure 3A).[37] Uptake via SLC38A1 and A2 can be distinguished from uptake via SLC1A5 by use of the SLC38-competitive substrate methylaminoisobutyric acid (MeAIB). Hence, uptake via SLC1A5 would be unaffected by competition with MeAIB, whereas uptake via SLC38A1 and A2 would be impaired. Figure 3D shows that HPG and AHA uptake is competitively blocked by alanine with IC_{50} values of 825 and 540 μM, respectively. In contrast, MeAIB did not inhibit uptake at any concentration assayed. Lysine was used as a control amino acid that is not a substrate for either SLC1A5 or SLC38A1/2 and also did not inhibit AHA or HPG uptake (Figures 3D and 3E). Taken together, these data argue that SLC1A5 is the predominant transporter involved in HPG and AHA transport into activated T cells.

To confirm the results obtained in murine T cells, we performed similar uptake experiments for murine cDC1 and human NK92 cells. The data show that competition with alanine reduced the uptake of HPG into cDC1s as measured by flow cytometry (Figure 3F). The ImmGen RNA sequencing (RNA-seq) dataset GEO: GSE127267 shows that SLC1A5 is the most highly expressed glutamine transporter in cDC1s (Figure S2B). Similarly, RNA-seq data from GEO: GSE26876 show that SLC1A5 is expressed in NK92 cells (Figure S2C). Consistent with SLC1A5-mediated uptake of HPG into NK92 cells, the data showed that the uptake of HPG was inhibited by competition with alanine (Figure 3G).

Uptake of AHA and HPG uptake into activated CD8 and CD4 T cells is also competitively inhibited by increasing glutamine concentrations with an IC_{50} value of <1 mM (Figures 4A and S3A). Glutamine also potently competes for HPG uptake into cDC1s and NK92 cells, providing strong evidence that these bioorthogonal amino acids are accurate reporters of glutamine

(D and E) AHA and HPG uptakes, performed as in (A), in the presence of increasing concentrations of alanine, lysine, or MeAIB. Data are background adjusted MFI values for a representative experiment (D) and pooled data (E) showing competition with 3.3 mM of alanine, lysine, or MeAIB.
(F and G) Representative histogram (left) and pooled data (right) showing 2 min HPG (200 μM) uptake into splenic cDC1^{Xcr1+} ± 5 mM alanine (F) or NK92 cells ± increasing alanine concentrations (G).
Data are mean ± SEM of 4 (D and E, top), 2 (D and E, bottom), 3 (C and G), or 5 (F) independent experiments; data points represent biological replicates. In (B), data are mean ± SD of technical triplicates and representative of 3 independent experiments. Data are analyzed using a two-way ANOVA (B) or one-way ANOVA (E) with Tukey post-tests or a one-sample t test (against a value of 1) (F) (*$p < 0.05$; **$p < 0.01$; ***$p < 0.001$).

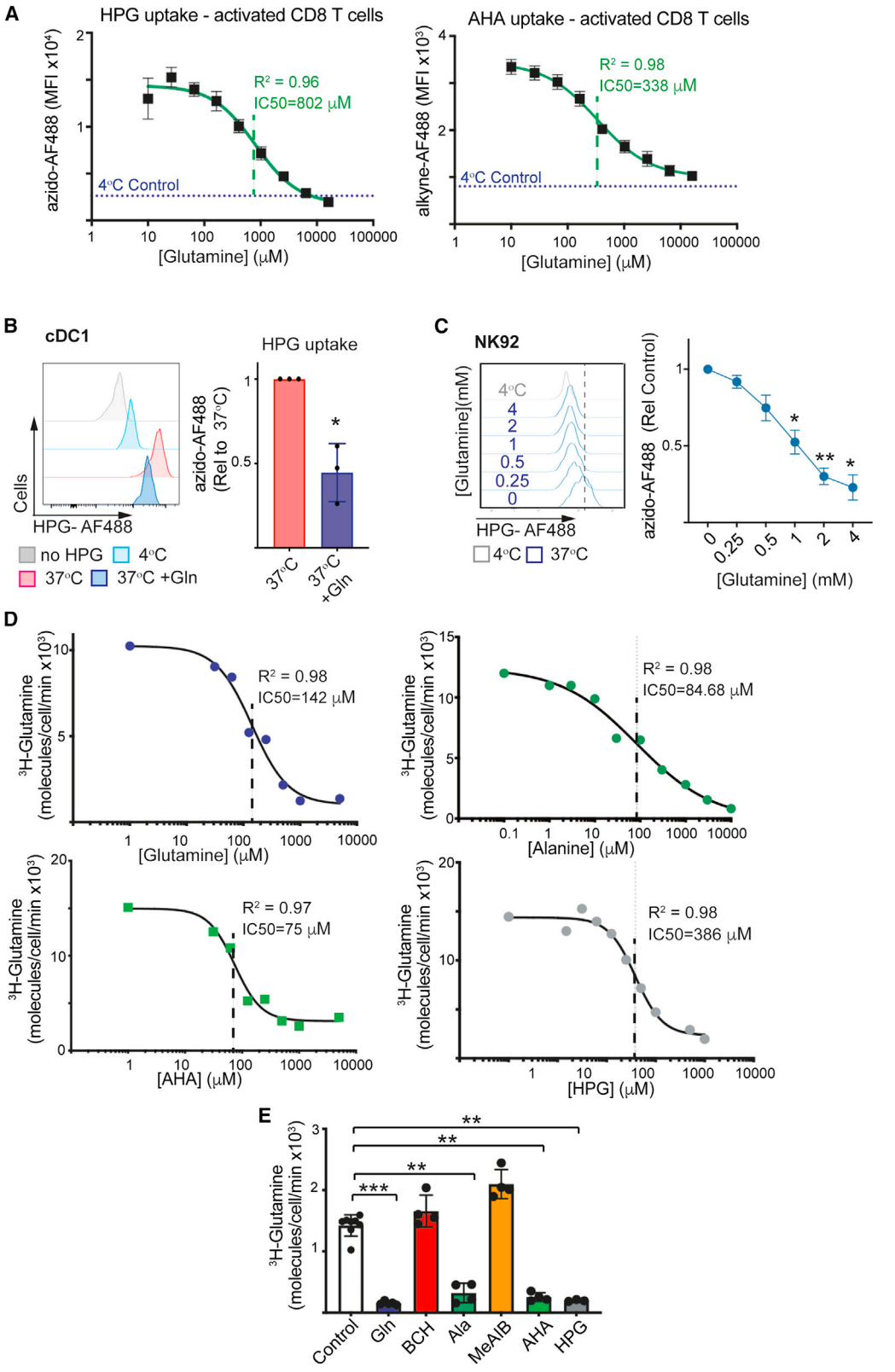

(legend on next page)

uptake (Figures 4B and 4C). The gold-standard approach for measuring transporter-mediated nutrient uptake is to use radiolabeled substrates. Therefore, we used this approach to provide definitive evidence of SLC1A5-mediated uptake of HPG and AHA. Firstly, we confirmed that both alanine and glutamine would compete with radiolabeled glutamine (^{3}H-glutamine) for uptake in activated CD8 T cells. For these radiolabeled uptakes, we used *in-vitro*-generated interleukin-2 (IL-2)-maintained effector CD8 T cells, cytotoxic T cells (CTLs). CTLs can be expanded into a large, homogeneous population, which is appropriate for this population-based uptake approach. Furthermore, as with T cell receptor (TCR) activated T cells, SLC1A5 is the predominant glutamine transporter expressed by IL-2-maintained CTLs.[37] The data in Figure 4D show that glutamine effectively competes for the uptake of ^{3}H-glutamine into CTLs, with an IC_{50} of 142 μM, while alanine competes for ^{3}H-glutamine uptake with an IC_{50} of 85 μM. These values are in line with previously published glutamine affinities for SLC1A5/ASCT2.[38] Next, we challenged the specificity of HPG and AHA uptake by determining whether each biorthogonal amino acid could act as competitive inhibitor to block the uptake of ^{3}H-glutamine. We found that both HPG (IC50 of 386 μM) and AHA (IC50 of 74 μM) compete for ^{3}H-glutamine uptake. In contrast, the uptake of ^{3}H-glutamine was not affected by the presence of 2-aminobicyclo-(2,2,1)-heptane-2-carboxylic acid (BCH) or MeAIB, which are competitive substrates for SLC7A5 and SLC38A1/2, respectively (Figure 4E).

We also tested another biorthogonal amino acid that we originally predicted would be taken up by SLC1A5, as it was reported to be an isostere of glutamine. Interestingly, this α-azido-glutamine was not taken up by activated T cells. It required very high concentrations (>1 mM) and long (>15 min) incubation for any signal to be seen (Figures S3B and S3C). Therefore, we conclude that α-azido-glutamine is not a suitable substrate for use as a reporter for glutamine uptake capacity with this assay.

Taken together, our findings provide an easy procedure to assess which cells support their function via SLC1A5-mediated uptake of amino acids in a sensitive single-cell assay, wherein click-functionalized reporter molecules, with either an azide or an alkyne group, can be introduced to match the preferred detection method.

Resolving SLC1A5 uptake capacity in complex immune populations

One barrier to applying this approach for use in complex multiparametric flow cytometry analysis is the fact that copper-click chemistry has the potential to significantly quench the fluorescence of protein fluorophores, such as phycoerythrin (PE) and peridinin-chlorophyll-protein (PerCP), thereby significantly reducing the multiplexing power of this assay.[39,40]

We confirmed that copper sulfate, especially in combination with sodium ascorbate (the "click mix") significantly quenches PE, PE-Cy7, and PerCP fluorescent signals (Figures 5A and 5B). Addition of the Cu(I)-stabilizing ligand Tris(3-hydroxypropyltriazolylmethyl)amine (THPTA)[41] and aminoguanidine, sometimes used to prevent unwanted side reactions,[41,42] was able to restore the signal (Figures 5B and 5C), plateauing at 160 mM aminoguanidine (Figure 5C). Neither the click mix nor increasing aminoguanidine concentrations affected the fluorescent signals for fluorescein isothiocyanate (FITC) or APC (Figure 5C). Preservation of the signal worked best when the click-mix components were prepared fresh for the experiment (Figure 5D). A simplified overview of the workflow can be found in Figure S4.

We next analyzed murine thymocytes directly *ex vivo*. T cell development occurs in the thymus and involves tightly regulated stages of biosynthesis, proliferation, and contraction. Conventional thymocyte populations are categorized according to their expression of CD4 and CD8. Early T cell progenitors do not express CD4 or CD8 and are termed double-negative (DN) thymocytes. Thymocytes that successfully express a functional pre-TCR at the DN3 to DN4 transition undergo robust expansion and differentiate into CD4, CD8 double-positives (DPs). Only a small fraction of DP thymocytes are selected for further differentiation to generate mature CD4 or CD8 T cells.

As very little is known about the nutrient uptake of these different thymocyte populations, we used our bioorthogonal uptake assay to interrogate SLC1A5-mediated uptake capacity of thymocytes. The overall HPG uptake of total thymocytes is low (Figures 6A and S5A). However, there is substantial heterogeneity, with a small proportion of thymocytes that have high HPG uptake, which is sensitive to alanine competition and inhibited at 4°C (Figures 6A and S5A). Subgating reveals that HPG uptake levels are distinct for each thymocyte subset (Figures 6B and 6C). Uptake into DN thymocytes is high but heterogeneous, whereas uptake into DP thymocytes is low, consistent with the low metabolic demands known for the DP population (Figures 6B, 6C, and S5A). Uptake into CD8 single positive (CD8SP) or CD4SP was intermediate between DN and DP thymocytes (Figures 6C and S5A). The heterogeneity within DN thymocytes was further probed through separating out DN3 and DN4 thymocytes based on the expression of CD25 and CD44. Large metabolic changes occur as thymocytes transition from DN3 to DN4, as the thymocytes undergo robust growth and

Figure 4. HPG and AHA report glutamine transport capacity in immune cells

(A) Activated (anti-CD3/CD28 treated; 24 h) CD8 T cells were provided HPG (400 μM) or AHA (100 μM) with increasing concentrations of glutamine. Background adjusted MFI values are shown. Blue line indicates signal at 4°C control.

(B and C) Representative histogram (left) and pooled data (right) showing 2 min HPG (200 μM) uptake into splenic $cDC1^{Xcr1+}$ ± 5 mM glutamine (B) or NK92 cells ± increasing glutamine concentrations (C). 4°C controls also shown.

(D and E) ^{3}H-glutamine uptake in effector cytotoxic CD8 T cells (CTLs) showing representative experiment in the presence of increasing concentrations of glutamine, alanine, AHA, and HPG (D) and pooled data for uptake ± 5 mM multiple competitive substrates.

(A) Data are representative of 3 independent experiments (mean ± SD, technical triplicates). Data are representative of (B–D) 3 biological replicates, (B and C) mean ± SEM. (E) Data are mean ± SD 2 independent experiments performed in duplicate. Data are analyzed using (B and C) one-sample t tests (against a value of 1) and (E) a one-way ANOVA with a Dunnet's post-test (*$p < 0.05$; **$p < 0.01$; ***$p < 0.001$).

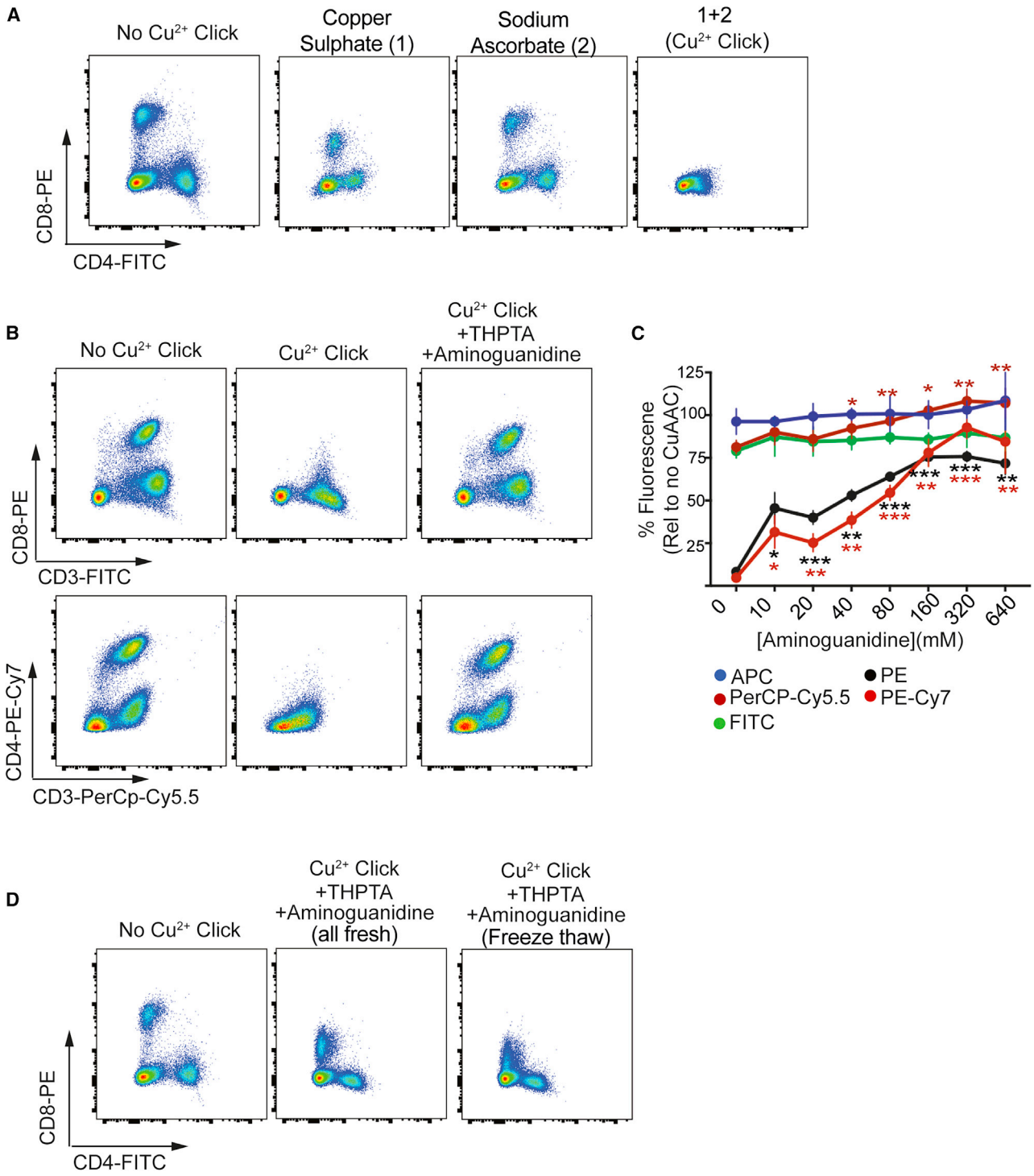

Figure 5. Fine-tuning the click mix to allow PE-/PerCP-based fluorophores in antibody panels

(A) Splenocytes were stained with CD4-FITC and CD8-PE and then incubated for 1 h with PBS (no click), 1 mM copper sulfate (1), 10 mM sodium ascorbate (2), or both together (click mix).

(B) Splenocytes were stained with CD3-FITC and CD8-PE or CD4-PE-Cy7 and CD3-PerCp-Cy5.5 and then incubated with the click mix for 1 h ± THPTA (1 mM) and aminoguanidine (160 mM).

(C) Data showing fluorescence signals of fluorophores incubated for 1 h with the click mix plus THPTA (1 mM) and with increasing concentrations of aminoguanidine (1–640 mM).

(legend continued on next page)

proliferation.[43] In agreement, the data show large increases in SLC1A5-mediated uptake in these proliferative DN4 thymocytes (Figure 6D). This analysis resolved clear differences in the SLC1A5 uptake capacity of thymocyte subpopulations that closely align to the mRNA expression pattern of SLC1A5 as reported on ImmGen (Figures 6E and S5A).

Finally, we probed the glutamine transporter uptake patterns within splenocytes when provided HPG directly *ex vivo* and combined with multiparametric flow cytometry to identify immune cell populations. The staining panel used identified T cells^{CD3+}, B cells^{CD19+}, and multiple antigen-presenting cells including plasmacytoid DC^{CD317+}, monocytes$^{CD11c-/CD11b+}$, DC$^{CD11c+/CD11b+}$, and cDC1^{Xcr1+}.

The data show distinct patterns of HPG uptake with the highest levels identified in the cDC1^{Xcr1+}, as well as several unknown populations, which were not identified by the antibody panel used (Figure 6F).

Increased amino acid uptake often correlates with increased rates of protein translation. Puromycin can be used as a probe for quantifying the rate of protein synthesis, as it is incorporated into newly formed polypeptide chains in the ribosome.[6] This incorporation can be visualized with single-cell resolution when a bioorthogonal puromycin analog that contains an alkyne is used, O-propargyl-puromycin (OPP). The copper-catalyzed click reaction can then be used to attach a fluorophore to OPP. Importantly, this probe does not require transporters to enter the cell. We used this approach to measure protein synthesis rates in splenocytes and show that Xcr1$^+$ DCs have high rates of *de novo* protein synthesis, which is blocked by an inhibitor of protein synthesis, cycloheximide (Figure 6G).

One powerful aspect of using the copper-catalyzed click reaction to reveal amino acid uptake is that it can easily be multiplexed.[44,45] With this in mind, we investigated whether we could simultaneously measure amino acid uptake and protein synthesis rates in single cells. We used alkyne-AF488 to detect azide-modified AHA uptake and azide-AF594 to detect alkyne-OPP incorporation into nascent protein chains. As expected, cDC1^{Xcr1+} with high SLC1A5-mediated AHA uptake were the same cells that stained brightly for protein synthesis (Figures 6H and 6I). Importantly, inhibition of protein synthesis with cycloheximide had no effect on the rate of AHA uptake during the time frame of the assays, confirming that protein synthesis rates do not affect the measurement of SLC1A5-mediated amino acid uptake (Figures 6H and 6I). Two additional questions remained relating to whether the addition of OPP and AHA together would affect the magnitude of the signals observed with either alone. The data show that the measured signal for AHA uptake was not affected by the addition of OPP (Figures 6J and 6L) and that the addition of AHA does not affect the measured signal for OPP incorporation (Figures 6K and 6L). We also performed this double-click assay for SLC1A5-mediated uptake and protein synthesis in human NK92 cells, confirming the versatility of these assays (Figures S6A and S6B).

Altogether, the data presented in Figure 6 highlight the potential for using bioorthogonal amino acid uptake assays to reveal metabolic features of *ex vivo* immune cells that were, until now, unreachable.

Tracking SLC1A5 uptake capacity *in vivo*

Many metabolic measurements made *in vitro* do not faithfully reflect immune cell metabolism, as it occurs *in vivo*.[46] *In vivo* application of HPG and AHA has previously been described either through muscular injection (xenopus) or dietary uptake (murine) or in environmental water (zebrafish) to label proteins.[47–49] To track *in vivo* HPG uptake during immune activation, we injected CPG (unmethylated-cytosine-phosphate-guanine) plus ovalbumin (OVA) subcutaneously into the ankle of OTI TCR transgenic mice (which have transgenic expression of an OVA-specific TCR), waited for 24 h, and then injected either HPG or PBS into the same mice by the same route. After waiting 40 min to permit HPG drainage into the lymph node and uptake into immune cells, the mice were sacrificed, and the draining popliteal lymph nodes (PLN) harvested. The cervical LNs (CLNs) were harvested as control LNs, distal to the site of injection (Figure 7A). Cells recovered from the CLNs showed no signal in the mice receiving HPG above mice receiving PBS injection (Figures 7A and 7B). In contrast, in cells recovered from the draining PLNs, there was a clear and significant increase in fluorescence in mice receiving HPG versus PBS. These data show that the immune cells in the draining, but not distal, LNs are exposed to HPG (Figures 7B and 7C). CD8 T cells in an OTI TCR transgenic mouse express a TCR specific for the OVA-derived peptide SIINFEKL. Injection of CPG/OVA primes antigen-presenting cells to take up and process OVA, migrate, and present the OVA-derived peptides to T cells in the proximal LNs, resulting in T cell activation. The CLNs have low numbers of activated T cells, based on the expression of the early activation marker CD69 (Figure 7D). In contrast, the PLN contains a large population of CD69$^+$ CD8 T cells (Figure 7D). Interrogation of the HPG uptake shows there was significant HPG uptake in CD69$^+$ CD8 T cells within the PLN (Figures 7D and 7E). CPG will also act upon other immune cells such as B cells. Indeed, there was increased expression of CD69 in some B cells in the PLN, but not the CLN, and these activated B cells also show enhanced uptake of HPG (Figures 7D and 7E). To exclude the possibility that the increased HPG signal is due to increased autofluorescence of larger cells, we measured the HPG uptake of CD69$^+$ activated CD8 T cells that had increased in size as determined by forward scatter (FSC-A^{high}) from mice that received HPG and from those that had received PBS (Figure 7F). The data show a substantial increase in HPG uptake signal into CD69$^+$ FSC-A^{high} CD8 T cells compared with the matched PBS controls (Figure 7F). Importantly, the HPG uptake

(D) Splenocytes stained with CD4-FITC and CD8-PE and then incubated with PBS (no click) or click mix + THPA (1 mM) + aminoguanidine (160 mM) prepared fresh or after multiple freeze thaws.

Data are mean ± SEM (C) or are representative (A, B, and D) of 4 independent experiments. Data are analyzed using a two-way ANOVA with a Dunnet's post-test (*p < 0.05; **p < 0.01; ***p < 0.001).

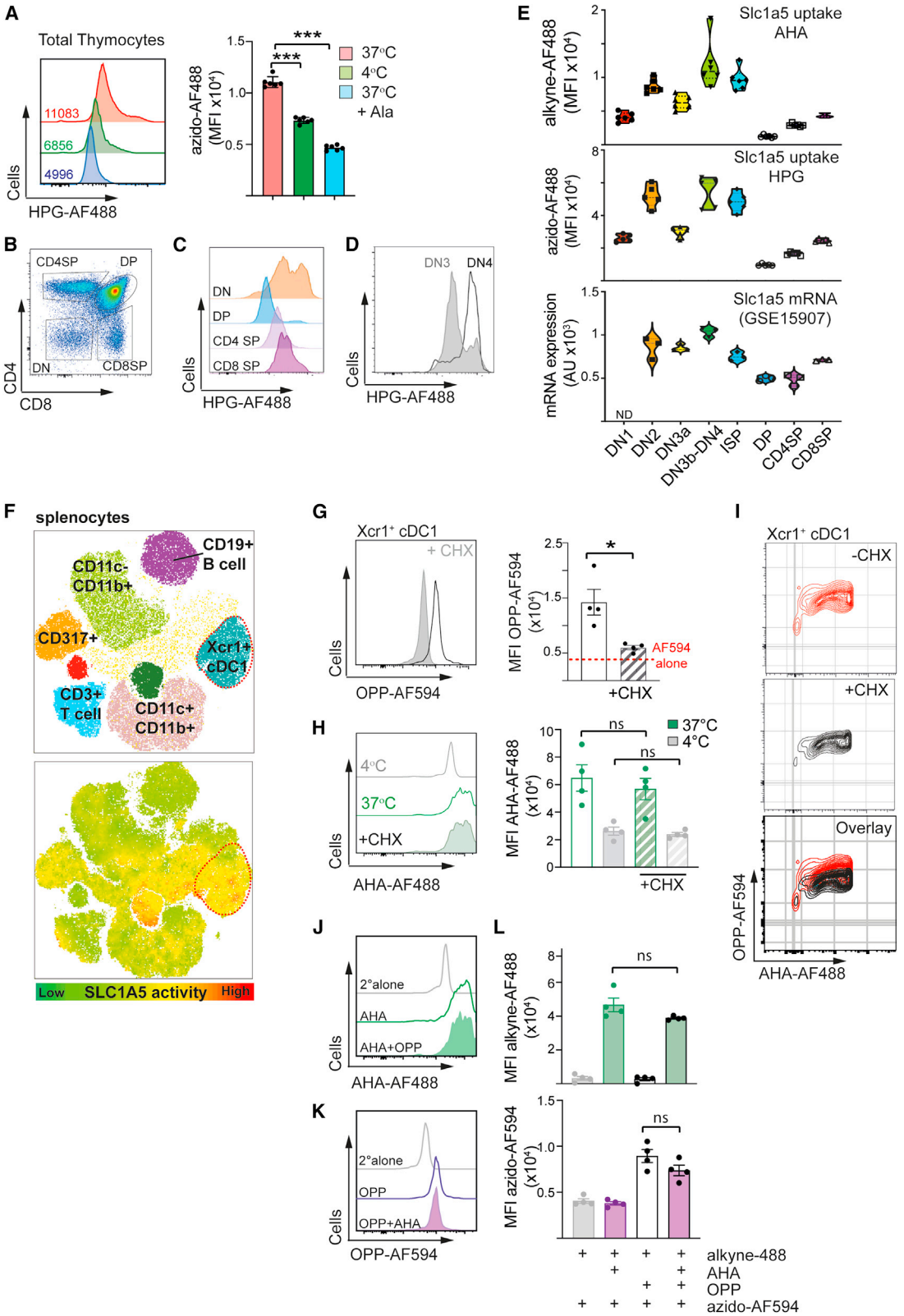

(legend on next page)

into the naive CD8 T cells, as determined by $CD69^{-}$ and FSC-A^{low} profiles, was significantly less that the activated $CD69^{+}$ FSC-A^{high} CD8 T cells (Figure 7G).

The *in vitro* and *ex vivo* data described herein define the regulated uptake of AHA and HPG in immune cells as being through a sodium-dependent, alanine- and glutamine-sensitive transporter. These biophysical parameters, in combination with transporter expression data from quantitative mass spectrometry, support AHA and HPG transport through SLC1A5 (ASCT2). Furthermore, we show that *in vivo* immune stimulation and subsequent *in vivo* HPG loading identifies HPG uptake in activated CD8 T cells. Together, these data demonstrate that *in vivo* HPG uptake, followed by *ex vivo* click resolution, can be used to identify cell populations with increased capacity of SLC1A5-mediated transport.

DISCUSSION

It is now clear that the metabolic features of immune cells are substantially altered after *in vitro* culture compared with those of immune cells *in vivo*.[46] This highlights the importance of studying immune metabolism *in vivo* or directly *ex vivo*. However, the lack of robust technologies to measure metabolic fluxes at a single-cell level represents a barrier preventing such *in vivo*, or directly *ex vivo*, analysis. This barrier is limiting our understanding of the metabolic demands, constraints, and heterogeneity within complex immune populations.

The research described herein provides a robust assay for amino acid transport through SLC1A5, the predominant glutamine transporter expressed in many immune cells (https://www.immgen.org and immpres.co.uk).[37] Glutamine acts as both a fuel for energy generation and a carbon source for biosynthesis. Through using radiolabeled uptake competition, Na^{+} dependence, and substrate competition approaches, we demonstrate that AHA and HPG are taken up by primary murine T cells and cDC1s and by human NK92 cells through SLC1A5. This assay is unique, as transport occurs first, followed by the attachment of a fluorophore to the bioorthogonal amino acid inside the cell using click chemistry. This innovative approach underpins the accuracy of this assay by avoiding the pitfalls common to other nutrient uptake assays based on assuming that transporter fidelity is retained with bulky fluorophores, such as with 2NBDG.[16]

Harnessing the single-cell resolution of this metabolic assay allowed the measurement of SLC1A5 amino acid flux in various thymocyte subsets. The uptake capacity of the thymocyte subsets was found to correlate closely with the expression pattern of SLC1A5 mRNA shown in the ImmGen dataset GEO: GSE15907. Clear heterogeneity in glutamine uptake capacity was also observed in immune cell subsets within the spleen, highlighting that DC1s have high SLC1A5-mediated uptake compared with other splenic lymphocyte populations.

We further expanded our interrogation of these cells by combining our new SLC1A5 uptake assay with measuring protein synthesis. This double-click assay revealed that cDC1 splenic cells that had high SLC1A5 transport capacity also showed high protein synthesis levels. Furthermore, during the time frame of this assay, inclusion of the bioorthogonal uptake amino acids had no impact on the rate of protein translation, nor did inhibition of translation with cycloheximide inhibit the uptake capacity of the transporter. These experiments also offer the tantalizing opportunity for a broader application of dual-click labeling. For instance, the AHA SLC1A5 uptake assay could be combined with an ethynyldeoxyuridine (EdU)-based click assay to correlate amino acid uptake to cell division[50] or the uptake of any of the other available alkyne-containing biomolecules.[51]

Finally, we demonstrate robust *in vivo* uptake of the bioorthogonal amino acid HPG at the single-cell level, previously not achievable using radiolabeled whole-cell populations.

Figure 6. Resolving SLC1A5 uptake capacity in complex immune populations

Thymocytes (A–E) or splenocytes (F and H–K) were provided HPG (400 μM) or AHA (100 μM) for 2 min at 4°C or 37°C and then fixed, and an AF488 fluorophore was conjugated with a copper- click reaction.

(A) HPG uptake into total thymocytes ± alanine (5 mM).

(B) Gating strategy to separate thymocytes based on CD4 and CD8 expression.

(C and D) HPG uptake into DN, DP, CD4SP, and CD8SP thymocytes (C) and following further subgating into DN3 ($CD25^{+}$ $CD44^{-}$) and DN4 ($CD25^{-}$ $CD44^{-}$) populations (D).

(E) HPG (top) and AHA (middle) uptake MFI (37°C–4°C) in thymocytes subsets, aligned with SLC1A5 mRNA expression data (bottom) from GEO: GSE15907 (Immgen.org). Each data point represents a biological replicate.

(F) Dimensionality reduction using t-distributed stochastic neighbor embedding (t-SNE) was performed on splenocytes for HPG uptake. Top panel shows splenocytes population including $CD11c^{+}MHCII^{+}XCR1^{+}CD11b^{-}$ cDC1s; $CD11c^{+}MHCII^{+}XCR1^{-}CD11b^{+}$ cDC2s; $CD11c^{int}CD317^{+}SiglecH^{+}$ pDCs; $CD3^{+}CD19^{-}$ T cells; and $CD19^{+}CD3^{-}$ B cells. Bottom panel shows the corresponding HPG uptake.

(G) Protein synthesis rates were measured by providing splenocytes with the puromycin analogue OPP (25 μM) ± the protein synthesis inhibitor cycloheximide (CHX; 100 μg/mL) for 20 min. Cells were then fixed, and an azide-AF594 fluorophore was conjugated with a copper-click reaction. Histogram (left) and pooled data (right) showing protein synthesis rates in $cDC1^{Xcr1+}$ with AF594 background indicated (red line).

(H) Histogram (left) and pooled MFI data (right) showing AHA uptake into $cDC1^{Xcr1+}$ ± CHX (100 μg/mL).

(I–K) To measure SLC1A5-mediated AHA uptake and protein synthesis rates concurrently, $cDC1^{Xcr1+}$ were cultured with OPP (25 μM, 20 min, 37°C) with AHA added for the final 2 min of this incubation.

(I) AHA uptake and OPP incorporation in $cDC1^{Xcr1+}$ ± CHX (100 μg/mL).

(J and K) Histogram of AHA uptake (J) or OPP incorporation (K) in $cDC1^{Xcr1+}$ when performed alone or concurrently.

(L) Pooled data for AHA uptake (top) or OPP incorporation (bottom) corresponding to (J) and (K).

(A–E) Data are representative or mean ± SEM of 2 individual experiments and 6 biological replicates. (F) Data are representative of 3 biological replicates. (G–L) Data are mean ± SEM or are representative of 2 individual experiments and 4 biological replicates. Data are analyzed using a Student's t test (G) or one-way ANOVA with a Sidak's post-test (A, H, and L) (*$p < 0.05$; ***$p < 0.001$).

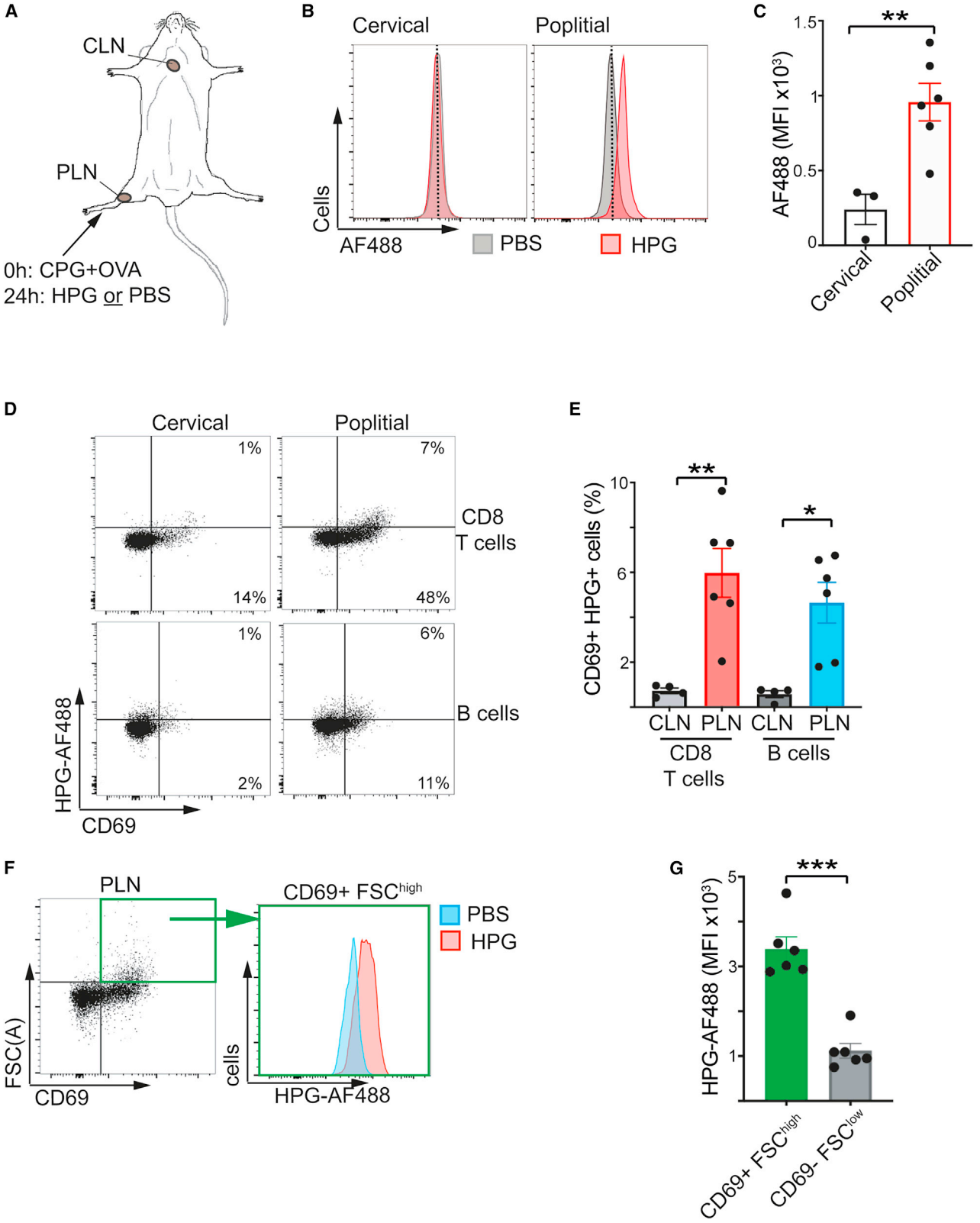

(legend on next page)

Together, these data demonstrate the power of this novel metabolic analysis in identifying differences in the metabolic activities of immune cells in complex populations.

This work has validated two distinct bioorthogonal amino acids as substrates for SLC1A5. AHA contains an azide to allow it to be visualized using an alkyne-fluorophore, while HPG contains an alkyne and can be visualized using an azide-fluorophore. This provides flexibility, where SLC1A5 flux analysis can be multiplexed to other assays that utilize bioorthogonal chemical reactions with a different bioorthogonal structure. This would involve a double-copper-click reaction using two separate fluorophores, one with an azide and the other with an alkyne, as demonstrated by our combining *azide*-containing AHA uptake with an *alkyne*-puromycin to monitor protein synthesis. Similarly, as additional assays of nutrient transporters become available, using this bioorthogonal strategy, it will become possible to measure two nutrient uptake fluxes simultaneously into a single cell. Altogether, our glutamine uptake assay with single-cell resolution (QUAS-R) represents a powerful addition to the ever-growing single-cell metabolic toolkit.

Limitations of the study

The key concept that underpins this work is that the alkyne-/azide-modified amino acids AHA and HPG "mimic" Gln to the SLC1A5 transporter. This may, however, not always be the case. For broadening of the scope of the reaction to other amino acids, such as the recently reported alkyne-threonine analogues,[52] the optimization and transporter specificity will have to be reevaluated for each species, as the data in this article show that no easy structure-uptake relationship can be drawn. These limitations have also restricted us to the use of the copper-catalyzed click conjugation,[53] which is hampered by its use of a toxic catalyst. Whereas some reaction conditions have been described that minimize this toxicity in a variety of cell lines,[54] we have found that great care has to be taken when applying these reactions to live primary immune cell populations.[55] Alternative live-cell-compatible bioorthogonal amino acids have also been described[56]; however, to date, they tend to give weaker signal-to-noise ratios and require long reaction times. It is also important to note that the signal reports on the uptake capacity of the cells but cannot distinguish ultimate anabolic destination of these amino acids.

Furthermore, some immune cells, such as immature cDC1s, may actively uptake material through transporter-independent mechanisms such as pinocytosis. Indeed, it is worth noting in these cells that the level of HPG uptake in the presence of competition with alanine or glutamine does not come down to that of the 4°C control, suggesting that the difference in fluorescence between the competition control and the 4°C control might reflect uptake by transporter-independent mechanisms. This highlights the importance of including the correct controls for all experiments.

STAR★METHODS

Detailed methods are provided in the online version of this paper and include the following:

- KEY RESOURCES TABLE
- RESOURCE AVAILABILITY
  - Lead contact
  - Materials availability
  - Data and code availability
- EXPERIMENTAL MODEL
  - Mice
  - NK92 cell culture
- METHOD DETAILS
  - T cell isolation and activation
  - *In vivo* DC expansion
  - Bioorthogonal amino acid uptake by flow cytometry
  - Click chemistry
  - Measuring protein synthesis
  - Double click assay using OPP and AHA
  - Flow cytometry
  - Flow cytometry antibodies
  - Spleen cDC staining panel
  - Thymocyte staining panel
  - OPP staining panel
  - Confocal microscopy
  - Radiolabeled ^{3}H-glutamine uptake
  - *In vivo* administration of HPG
- QUANTIFICATION AND STATISTICAL ANALYSIS

SUPPLEMENTAL INFORMATION

Supplemental information can be found online at https://doi.org/10.1016/j.celrep.2023.112828.

Figure 7. *In vivo* HPG uptake into activated CD8 T cells

(A) OTI transgenic mice were injected with CPG (25 μg) plus OVA (25 μg) in 25 μL PBS by subcutaneous injection in the ankle. After 24 h, the mice were administered HPG (25 μL 10 mg/mL HPG) or PBS by subcutaneous injection at the same site. After 40 min, the mice were sacrificed, and the draining popliteal lymph nodes (PLNs) and distal cervical lymph nodes (CLNs) were harvested. HPG uptake was visualized by *ex vivo* attachment of azido-AF488 with Cu^{2+} click reaction.

(B and C) Total cells from the CLNs and PLNs were analyzed for AF488 fluorescence (B) and quantified (MFI HPG − MFI PBS) (C).

(D) CD8 T cells (top) and B cells (below) were analyzed for CD69 expression and fluorescence in the AF488 channel in CLNs and PLNs.

(E) Pooled data showing the percentage of activated cells with increased HPG uptake in CLNs and PLNs.

(F) CD8 T cells from PLNs were gated on activated ($CD69^{+}$) T cells that were engaging in blastogenesis (FSC^{high}) (green box). Fluorescence in the AF488 channel was compared for activated T cells in mice that received HPG versus those that received PBS.

(G) The HPG-specific signal for $CD69^{+}FSC^{high}$ and $CD69^{-}FSC^{low}$ CD8 T cells was quantified by subtracting the MFI for the PBS condition from the MFI for the HPG condition.

Data are representative (B, D, F) or are mean ± SEM (C, E, and G) of 6 individual PLNs and 3–4 individual CLNs. Data are analyzed using a Student's t test (C and G) or a one-way ANOVA with a Sidak's post-test (E) (*$p < 0.05$; **$p < 0.01$; ***$p < 0.001$).

ACKNOWLEDGMENTS

We would like to thank members of the Cantrell, Finlay, and Van Kasteren labs for constructive advice and reading of the manuscript. This research was supported by ERC CoG 770769 (D.F., L.P., G.D., S.O'S.) and ERC CoG 865175 (S.V.K.), and L.S. was supported by a Wellcome Trust Principal Research Fellowship, awarded to Doreen Cantrell (205023/Z/16/Z).

AUTHOR CONTRIBUTIONS

Conceptualization, L.P., S.V.K., D.F., and L.S.; investigation, L.P., G.D., S.O'S., E.W., S.V.K., D.F., and L.S.; methodology and writing – review and editing, L.P., G.D., S.V.K., D.F., and L.S.

DECLARATION OF INTERESTS

The authors declare no competing interests.

INCLUSION AND DIVERSITY

We support inclusive, diverse, and equitable conduct of research.

Received: October 26, 2022
Revised: May 26, 2023
Accepted: July 3, 2023
Published: July 19, 2023

REFERENCES

1. O'Neill, L.A.J., Kishton, R.J., and Rathmell, J. (2016). A guide to immunometabolism for immunologists. Nat. Rev. Immunol. *16*, 553–565. https://doi.org/10.1038/nri.2016.70.
2. Assmann, N., and Finlay, D.K. (2016). Metabolic regulation of immune responses: therapeutic opportunities. J. Clin. Invest. *126*, 2031–2039. https://doi.org/10.1172/JCI83005.
3. Bader, J.E., Voss, K., and Rathmell, J.C. (2020). Targeting Metabolism to Improve the Tumor Microenvironment for Cancer Immunotherapy. Mol. Cell *78*, 1019–1033. https://doi.org/10.1016/j.molcel.2020.05.034.
4. Leone, R.D., Zhao, L., Englert, J.M., Sun, I.M., Oh, M.H., Sun, I.H., Arwood, M.L., Bettencourt, I.A., Patel, C.H., Wen, J., et al. (2019). Glutamine blockade induces divergent metabolic programs to overcome tumor immune evasion. Science *366*, 1013–1021. https://doi.org/10.1126/science.aav2588.
5. Marchingo, J.M., Sinclair, L.V., Howden, A.J., and Cantrell, D.A. (2020). Quantitative analysis of how Myc controls T cell proteomes and metabolic pathways during T cell activation. Elife *9*, e53725. https://doi.org/10.7554/eLife.53725.
6. Sinclair, L.V., Howden, A.J., Brenes, A., Spinelli, L., Hukelmann, J.L., Macintyre, A.N., Liu, X., Thomson, S., Taylor, P.M., Rathmell, J.C., et al. (2019). Antigen receptor control of methionine metabolism in T cells. Elife *8*, e44210. https://doi.org/10.7554/eLife.44210.
7. Howden, A.J.M., Hukelmann, J.L., Brenes, A., Spinelli, L., Sinclair, L.V., Lamond, A.I., and Cantrell, D.A. (2019). Quantitative analysis of T cell proteomes and environmental sensors during T cell differentiation. Nat. Immunol. *20*, 1542–1554. https://doi.org/10.1038/s41590-019-0495-x.
8. Sinclair, L.V., Rolf, J., Emslie, E., Shi, Y.B., Taylor, P.M., and Cantrell, D.A. (2013). Control of amino-acid transport by antigen receptors coordinates the metabolic reprogramming essential for T cell differentiation. Nat. Immunol. *14*, 500–508. https://doi.org/10.1038/ni.2556.
9. Nakaya, M., Xiao, Y., Zhou, X., Chang, J.H., Chang, M., Cheng, X., Blonska, M., Lin, X., and Sun, S.C. (2014). Inflammatory T cell responses rely on amino acid transporter ASCT2 facilitation of glutamine uptake and mTORC1 kinase activation. Immunity *40*, 692–705. https://doi.org/10.1016/j.immuni.2014.04.007.
10. Geiger, R., Rieckmann, J.C., Wolf, T., Basso, C., Feng, Y., Fuhrer, T., Kogadeeva, M., Picotti, P., Meissner, F., Mann, M., et al. (2016). L-Arginine Modulates T Cell Metabolism and Enhances Survival and Anti-tumor Activity. Cell *167*, 829–842.e13. https://doi.org/10.1016/j.cell.2016.09.031.
11. Macintyre, A.N., Gerriets, V.A., Nichols, A.G., Michalek, R.D., Rudolph, M.C., Deoliveira, D., Anderson, S.M., Abel, E.D., Chen, B.J., Hale, L.P., and Rathmell, J.C. (2014). The glucose transporter Glut1 is selectively essential for CD4 T cell activation and effector function. Cell Metab. *20*, 61–72. https://doi.org/10.1016/j.cmet.2014.05.004.
12. Roy, D.G., Chen, J., Mamane, V., Ma, E.H., Muhire, B.M., Sheldon, R.D., Shorstova, T., Koning, R., Johnson, R.M., Esaulova, E., et al. (2020). Methionine Metabolism Shapes T Helper Cell Responses through Regulation of Epigenetic Reprogramming. Cell Metab. *31*, 250–266.e9. https://doi.org/10.1016/j.cmet.2020.01.006.
13. Laguerre, A., and Schultz, C. (2018). Novel lipid tools and probes for biological investigations. Curr. Opin. Cell Biol. *53*, 97–104. https://doi.org/10.1016/j.ceb.2018.06.013.
14. Reinfeld, B.I., Madden, M.Z., Wolf, M.M., Chytil, A., Bader, J.E., Patterson, A.R., Sugiura, A., Cohen, A.S., Ali, A., Do, B.T., et al. (2021). Cell-programmed nutrient partitioning in the tumour microenvironment. Nature *593*, 282–288. https://doi.org/10.1038/s41586-021-03442-1.
15. D'Souza, L.J., Wright, S.H., and Bhattacharya, D. (2022). Genetic evidence that uptake of the fluorescent analog 2NBDG occurs independently of known glucose transporters. PLoS One *17*, e0261801. https://doi.org/10.1371/journal.pone.0261801.
16. Sinclair, L.V., Barthelemy, C., and Cantrell, D.A. (2020). Single Cell Glucose Uptake Assays: A Cautionary Tale. Immunometabolism *2*, e200029. https://doi.org/10.20900/immunometab20200029.
17. Sinclair, L.V., Neyens, D., Ramsay, G., Taylor, P.M., and Cantrell, D.A. (2018). Single cell analysis of kynurenine and System L amino acid transport in T cells. Nat. Commun. *9*, 1981. https://doi.org/10.1038/s41467-018-04366-7.
18. Sletten, E.M., and Bertozzi, C.R. (2009). Bioorthogonal chemistry: fishing for selectivity in a sea of functionality. Angew Chem. Int. Ed. Engl. *48*, 6974–6998. https://doi.org/10.1002/anie.200900942.
19. Ramil, C.P., and Lin, Q. (2013). Bioorthogonal chemistry: strategies and recent developments. Chem. Commun. *49*, 11007–11022. https://doi.org/10.1039/c3cc44272a.
20. Bird, R.E., Lemmel, S.A., Yu, X., and Zhou, Q.A. (2021). Bioorthogonal Chemistry and Its Applications. Bioconjugate Chem. *32*, 2457–2479. https://doi.org/10.1021/acs.bioconjchem.1c00461.
21. Saxon, E., and Bertozzi, C.R. (2000). Cell surface engineering by a modified Staudinger reaction. Science *287*, 2007–2010. https://doi.org/10.1126/science.287.5460.2007.
22. Bertozzi, C.R. (2011). A decade of bioorthogonal chemistry. Acc. Chem. Res. *44*, 651–653. https://doi.org/10.1021/ar200193f.
23. Gao, X., and Hannoush, R.N. (2018). A Decade of Click Chemistry in Protein Palmitoylation: Impact on Discovery and New Biology. Cell Chem. Biol. *25*, 236–246. https://doi.org/10.1016/j.chembiol.2017.12.002.
24. Suazo, K.F., Park, K.Y., and Distefano, M.D. (2021). A Not-So-Ancient Grease History: Click Chemistry and Protein Lipid Modifications. Chem. Rev. *121*, 7178–7248. https://doi.org/10.1021/acs.chemrev.0c01108.
25. Buck, S.B., Bradford, J., Gee, K.R., Agnew, B.J., Clarke, S.T., and Salic, A. (2008). Detection of S-phase cell cycle progression using 5-ethynyl-2'-deoxyuridine incorporation with click chemistry, an alternative to using 5-bromo-2'-deoxyuridine antibodies. Biotechniques *44*, 927–929. https://doi.org/10.2144/000112812.
26. Jao, C.Y., and Salic, A. (2008). Exploring RNA transcription and turnover in vivo by using click chemistry. Proc. Natl. Acad. Sci. USA *105*, 15779–15784. https://doi.org/10.1073/pnas.0808480105.
27. Ignacio, B.J., Bakkum, T., Bonger, K.M., Martin, N.I., and van Kasteren, S.I. (2021). Metabolic labeling probes for interrogation of the

host-pathogen interaction. Org. Biomol. Chem. *19*, 2856–2870. https://doi.org/10.1039/d0ob02517h.

28. Chang, P.V., Prescher, J.A., Sletten, E.M., Baskin, J.M., Miller, I.A., Agard, N.J., Lo, A., and Bertozzi, C.R. (2010). Copper-free click chemistry in living animals. Proc. Natl. Acad. Sci. USA *107*, 1821–1826. https://doi.org/10.1073/pnas.0911116107.

29. Laughlin, S.T., Baskin, J.M., Amacher, S.L., and Bertozzi, C.R. (2008). In vivo imaging of membrane-associated glycans in developing zebrafish. Science *320*, 664–667. https://doi.org/10.1126/science.1155106.

30. Kiick, K.L., Saxon, E., Tirrell, D.A., and Bertozzi, C.R. (2002). Incorporation of azides into recombinant proteins for chemoselective modification by the Staudinger ligation. Proc. Natl. Acad. Sci. USA *99*, 19–24. https://doi.org/10.1073/pnas.012583299.

31. van Kasteren, S.I., Kramer, H.B., Jensen, H.H., Campbell, S.J., Kirkpatrick, J., Oldham, N.J., Anthony, D.C., and Davis, B.G. (2007). Expanding the diversity of chemical protein modification allows post-translational mimicry. Nature *446*, 1105–1109. https://doi.org/10.1038/nature05757.

32. Dieterich, D.C., Link, A.J., Graumann, J., Tirrell, D.A., and Schuman, E.M. (2006). Selective identification of newly synthesized proteins in mammalian cells using bioorthogonal noncanonical amino acid tagging (BONCAT). Proc. Natl. Acad. Sci. USA *103*, 9482–9487. https://doi.org/10.1073/pnas.0601637103.

33. Steward, K.F., Eilers, B., Tripet, B., Fuchs, A., Dorle, M., Rawle, R., Soriano, B., Balasubramanian, N., Copié, V., Bothner, B., and Hatzenpichler, R. (2020). Metabolic Implications of Using BioOrthogonal Non-Canonical Amino Acid Tagging (BONCAT) for Tracking Protein Synthesis. Front. Microbiol. *11*, 197. https://doi.org/10.3389/fmicb.2020.00197.

34. Dieterich, D.C., Lee, J.J., Link, A.J., Graumann, J., Tirrell, D.A., and Schuman, E.M. (2007). Labeling, detection and identification of newly synthesized proteomes with bioorthogonal non-canonical amino-acid tagging. Nat. Protoc. *2*, 532–540. https://doi.org/10.1038/nprot.2007.52.

35. Cueto, F.J., Del Fresno, C., Brandi, P., Combes, A.J., Hernández-García, E., Sánchez-Paulete, A.R., Enamorado, M., Bromley, C.P., Gomez, M.J., Conde-Garrosa, R., et al. (2021). DNGR-1 limits Flt3L-mediated antitumor immunity by restraining tumor-infiltrating type I conventional dendritic cells. J. Immunother. Cancer *9*, e002054. https://doi.org/10.1136/jitc-2020-002054.

36. Karsunky, H., Merad, M., Cozzio, A., Weissman, I.L., and Manz, M.G. (2003). Flt3 ligand regulates dendritic cell development from Flt3+ lymphoid and myeloid-committed progenitors to Flt3+ dendritic cells in vivo. J. Exp. Med. *198*, 305–313. https://doi.org/10.1084/jem.20030323.

37. Brenes, A.J., Hukelmann, J.L., Spinelli, L., Howden, A.J.M., Marchingo, J.M., Sinclair, L.V., Rollings, C., James, O.J., Phair, I.R., Matthews, S.P., et al. (2022). The Immunological Proteome Resource. Preprint at bioRxiv. https://doi.org/10.1101/2022.08.29.505666.

38. Scalise, M., Pochini, L., Console, L., Losso, M.A., and Indiveri, C. (2018). The Human SLC1A5 (ASCT2) Amino Acid Transporter: From Function to Structure and Role in Cell Biology. Front. Cell Dev. Biol. *6*, 96. https://doi.org/10.3389/fcell.2018.00096.

39. Bos, A.V., Erkelens, M.N., Koenders, S.T.A., van der Stelt, M., van Egmond, M., and Mebius, R.E. (2021). Clickable Vitamins as a New Tool to Track Vitamin A and Retinoic Acid in Immune Cells. Front. Immunol. *12*, 671283. https://doi.org/10.3389/fimmu.2021.671283.

40. Gaebler, A., Penno, A., Kuerschner, L., and Thiele, C. (2016). A highly sensitive protocol for microscopy of alkyne lipids and fluorescently tagged or immunostained proteins. J. Lipid Res. *57*, 1934–1947. https://doi.org/10.1194/jlr.D070565.

41. Hong, V., Presolski, S.I., Ma, C., and Finn, M.G. (2009). Analysis and optimization of copper-catalyzed azide-alkyne cycloaddition for bioconjugation. Angew Chem. Int. Ed. Engl. *48*, 9879–9883. https://doi.org/10.1002/anie.200905087.

42. van Elsland, D.M., Bos, E., de Boer, W., Overkleeft, H.S., Koster, A.J., and van Kasteren, S.I. (2016). Detection of bioorthogonal groups by correlative light and electron microscopy allows imaging of degraded bacteria in phagocytes. Chem. Sci. *7*, 752–758. https://doi.org/10.1039/c5sc02905h.

43. Kelly, A.P., Finlay, D.K., Hinton, H.J., Clarke, R.G., Fiorini, E., Radtke, F., and Cantrell, D.A. (2007). Notch-induced T cell development requires phosphoinositide-dependent kinase 1. EMBO J. *26*, 3441–3450. https://doi.org/10.1038/sj.emboj.7601761.

44. Bakkum, T., Heemskerk, M.T., Bos, E., Groenewold, M., Oikonomeas-Koppasis, N., Walburg, K.V., van Veen, S., van der Lienden, M.J.C., van Leeuwen, T., Haks, M.C., et al. (2020). Bioorthogonal Correlative Light-Electron Microscopy of Mycobacterium tuberculosis in Macrophages Reveals the Effect of Antituberculosis Drugs on Subcellular Bacterial Distribution. ACS Cent. Sci. *6*, 1997–2007. https://doi.org/10.1021/acscentsci.0c00539.

45. Bertheussen, K., van de Plassche, M., Bakkum, T., Gagestein, B., Ttofi, I., Sarris, A.J.C., Overkleeft, H.S., van der Stelt, M., and van Kasteren, S.I. (2022). Live-Cell Imaging of Sterculic Acid-a Naturally Occurring 1,2-Cyclopropene Fatty Acid-by Bioorthogonal Reaction with Turn-On Tetrazine-Fluorophore Conjugates. Angew Chem. Int. Ed. Engl. *61*, e202207640. https://doi.org/10.1002/anie.202207640.

46. Ma, E.H., Verway, M.J., Johnson, R.M., Roy, D.G., Steadman, M., Hayes, S., Williams, K.S., Sheldon, R.D., Samborska, B., Kosinski, P.A., et al. (2019). Metabolic Profiling Using Stable Isotope Tracing Reveals Distinct Patterns of Glucose Utilization by Physiologically Activated CD8(+) T Cells. Immunity *51*, 856–870.e5. https://doi.org/10.1016/j.immuni.2019.09.003.

47. Hinz, F.I., Dieterich, D.C., Tirrell, D.A., and Schuman, E.M. (2012). Non-canonical amino acid labeling in vivo to visualize and affinity purify newly synthesized proteins in larval zebrafish. ACS Chem. Neurosci. *3*, 40–49. https://doi.org/10.1021/cn2000876.

48. McClatchy, D.B., Ma, Y., Liu, C., Stein, B.D., Martínez-Bartolomé, S., Vasquez, D., Hellberg, K., Shaw, R.J., and Yates, J.R., 3rd. (2015). Pulsed Azidohomoalanine Labeling in Mammals (PALM) Detects Changes in Liver-Specific LKB1 Knockout Mice. J. Proteome Res. *14*, 4815–4822. https://doi.org/10.1021/acs.jproteome.5b00653.

49. Shen, W., Liu, H.H., Schiapparelli, L., McClatchy, D., He, H.Y., Yates, J.R., 3rd, and Cline, H.T. (2014). Acute synthesis of CPEB is required for plasticity of visual avoidance behavior in Xenopus. Cell Rep. *6*, 737–747. https://doi.org/10.1016/j.celrep.2014.01.024.

50. Salic, A., and Mitchison, T.J. (2008). A chemical method for fast and sensitive detection of DNA synthesis in vivo. Proc. Natl. Acad. Sci. USA *105*, 2415–2420. https://doi.org/10.1073/pnas.0712168105.

51. Patterson, D.M., Nazarova, L.A., and Prescher, J.A. (2014). Finding the right (bioorthogonal) chemistry. ACS Chem. Biol. *9*, 592–605. https://doi.org/10.1021/cb400828a.

52. Ignacio, B.J., Dijkstra, J., Garcia, N.M., Slot, E.F.J., Weijsten, M.J.v., Storkebaum, E., Vermeulen, M., and Bonger, K.M. (2022). THRONCAT: Efficient metabolic labeling of newly synthesized proteins using a bioorthogonal threonine analog. Preprint at bioRxiv. https://doi.org/10.1101/2022.03.29.486210.

53. Wang, Q., Chan, T.R., Hilgraf, R., Fokin, V.V., Sharpless, K.B., and Finn, M.G. (2003). Bioconjugation by copper(I)-catalyzed azide-alkyne [3 + 2] cycloaddition. J. Am. Chem. Soc. *125*, 3192–3193. https://doi.org/10.1021/ja021381e.

54. Li, S., Wang, L., Yu, F., Zhu, Z., Shobaki, D., Chen, H., Wang, M., Wang, J., Qin, G., Erasquin, U.J., et al. (2017). Copper-Catalyzed Click Reaction on/in Live Cells. Chem. Sci. *8*, 2107–2114. https://doi.org/10.1039/C6SC02297A.

55. Poulcharidis, D., Belfor, K., Kros, A., and van Kasteren, S.I. (2017). A flow cytometry assay to quantify intercellular exchange of membrane components. Chem. Sci. *8*, 5585–5590. https://doi.org/10.1039/c7sc00260b.

56. Lang, K., and Chin, J.W. (2014). Bioorthogonal reactions for labeling proteins. ACS Chem. Biol. *9*, 16–20. https://doi.org/10.1021/cb4009292.

57. Brenes, A.J., Lamond, A.I., and Cantrell, D.A. (2023). The Immunological Proteome Resource. Nat. Immunol. *24*, 731. https://doi.org/10.1038/s41590-023-01483-4.

58. Mach, N., Gillessen, S., Wilson, S.B., Sheehan, C., Mihm, M., and Dranoff, G. (2000). Differences in dendritic cells stimulated in vivo by tumors engineered to secrete granulocyte-macrophage colony-stimulating factor or Flt3-ligand. Cancer Res. *60*, 3239–3246.

59. Zhang, M.M., Tsou, L.K., Charron, G., Raghavan, A.S., and Hang, H.C. (2010). Tandem fluorescence imaging of dynamic S-acylation and protein turnover. Proc. Natl. Acad. Sci. USA *107*, 8627–8632. https://doi.org/10.1073/pnas.0912306107.

60. Kamala, T. (2007). Hock immunization: a humane alternative to mouse footpad injections. J. Immunol. Methods *328*, 204–214. https://doi.org/10.1016/j.jim.2007.08.004.

STAR★METHODS

KEY RESOURCES TABLE

REAGENT or RESOURCE	SOURCE	IDENTIFIER
Antibodies		
CD3ε (hamster anti-mouse, clone 145-2C11, pure, Ultra-LEAF)	BioLegend	Cat. #100340; RRID: AB_11149115
CD3ε (hamster anti-mouse, clone 145-2C11, APC)	BioLegend	Cat. # 100312; RRID: AB_312677
CD3ε (hamster anti-mouse, clone 145-2C11, FITC)	eBiosciences	Cat. #11-0031-85; RRID: AB_464882
CD4 (rat anti-mouse, clone GK1.5, PE-Cy7)	BioLegend	Cat. #100422; RRID: AB_312707
CD4 (rat anti-mouse/human, clone RM4-5, PE-Cy7)	BD Pharmingen	Cat. # 552775; RRID: AB_394461
CD4 (rat anti-mouse/human, clone RM4-5, APC)	eBioscience	Cat. #17-0042-83; RRID: AB_469324
CD8a (rat anti-mouse, clone 53–6.7, APC-Cy7)	BioLegend	Cat #100714; RRID: AB_312753
CD8a (rat anti-mouse, clone 53–6.7, PerCP-Cy5.5)	BD Pharmingen	Cat. #551162; RRID: AB_394081
CD11b (rat anti-mouse, clone M1/70, BV605)	BioLegend	Cat. #101257; RRID: AB_2565431
CD11b (rat anti-mouse, clone M1/70, PE)	eBioscience	Cat. #12-0112-81; RRID: AB_465546
CD11b (rat anti-mouse, clone M1/70, BV510)	BD Horizon	Cat. #562950; RRID: AB_2737913
CD11c (hamster anti-mouse, clone HL3, BV421)	BD Horizon	Cat. #562782; RRID: AB_2737789
CD16/32 (TrueStain FcX, rat anti-mouse, clone S17011E, pure)	BioLegend	Cat. #156604; RRID: AB_2783138
CD16/32 (FC block, rat anti-mouse, clone 2.4G2, pure)	BD Pharmingen	Cat. # 553142; RRID: AB_394656
CD19 (rat anti-mouse, clone 1D3, PE-Cy7)	BD Pharmingen	Cat. #552854; RRID: AB_394495
CD19 (mouse anti-mouse, clone MB19-1, PE)	eBioscience	Cat. #12-0191-83; RRID: AB_465578
CD19 (rat anti-mouse, clone 1D3, BV650)	BD Horizon	Cat. #563235; RRID: AB_2738085
CD24 (rat anti-mouse, clone M1/69, BV421)	BioLegend	Cat. #101825; RRID:AB_10901159
CD25 (rat anti-mouse, clone PC61, PerCP-Cy5.5)	BD Pharmingen	Cat. #561112; RRID: AB_394031
CD28 (hamster anti-mouse, clone 37.51, pure, Ultra-LEAF)	BioLegend	Cat. #102116; RRID: AB_11147170
CD44 (rat anti-mouse/human, clone IM7, PE-Cy7)	eBioscience	Cat. #25-0441-81; RRID: AB_469622
CD317 (PDCA1, rat anti-mouse, clone 927, BV650)	BioLegend	Cat. #127019; RRID: AB_2562477
B220 (CD45R, rat anti-mouse, clone RA3-6B2, PerCP-Cy5.5)	BioLegend	Cat. #103236; RRID: AB_893354
I-A/I-E (MHCII, rat anti-mouse, clone M5/114.15.2, APC)	BioLegend	Cat. #107613; RRID: AB_313328
I-A/I-E (MHCII, rat anti-mouse, clone M5/114.15.2, FITC)	eBioscience	Cat. #11-5321-82; RRID:AB_465232
I-A/I-E (MHCII, rat anti-mouse, clone M5/114.15.2, APC-eF780)	eBioscience	Cat. # 47-5321-82; RRID: AB_1548783
F4/80 (rat anti-mouse, clone Cl:A3-1, AF700	Bio-Rad	Cat. #MCA497A700; RRID: AB_844537
Gr-1 (Ly6G/Ly6C, rat anti-mouse, clone RB6-8C5, PE)	eBioscience	Cat. #12-5931-82; RRID: AB_466045

(*Continued on next page*)

Continued

REAGENT or RESOURCE	SOURCE	IDENTIFIER
NK1.1 (mouse anti-mouse, clone PK136, PE)	BD Pharmingen	Cat. # 557391; RRID: AB_396674
XCR1 (mouse anti-mouse/rat, clone ZET, BV785)	BioLegend	Cat. #148225; RRID: AB_2783119
XCR1 (mouse anti-mouse/rat, clone ZET, AF647)	BioLegend	Cat. #148213; RRID: AB_2564368
Chemicals, peptides, and recombinant proteins		
L-azidohomoalanine	Synthesized in house	CAS No. 942518-29-8
l-homopropargylglycine	Synthesized in house	CAS No. 942518-19-6
Tris-hydroxypropyltriazolylmethylamine	Synthesized in house	CAS No. 760952-88-3
Aminoguanidine	Cayman Chemicals	CAS No. 1937-19-5; Cat #81530
Copper(II) Sulfate pentahydrate	Sigma-Aldrich	CAS No. 7758-99-8; Cat #209198
AZDye 488 Alkyne	Click Chemistry Tools	Cat. No. #1277
AZDye 488 Azide	Click Chemistry Tools	Cat. No. #1275
AZDye 594 Azide	Click Chemistry Tools	Cat. No #1295
AZDye 647 Alkyne	Click Chemistry Tools	Cat. No. #1301
AZDye 647 Azide	Click Chemistry Tools	Cat. No. #1299
Sodium Ascorbate	Sigma-Aldrich	CAS No. 134-03-2; Cat. #A7631
DAPI	Invitrogen	Cat. #D1306
LIVE/DEAD™ Fixable Aqua Dead Cell Stain	Thermo	Cat. #L34957
Zombie Yellow™ Fixable Viability Kit	BioLegend	Cat. #423103
paraformaldehyde solution	Polysciences	Cat. #18814-20
O-propargyl-puromycin	Thermofisher	Cat# C10459
IL-12	Peprotech	#210-12
IL-2	Novartis	Proleukin
HBSS	Gibco	#24020
Bovine Serum Albumin	Sigma-Aldrich	#A9467
RPMI 1640	Sigma-Aldrich	#R5886
GlutaMAX	Gibco	#35050061
horse serum	Sigma-Aldrich	#H1270
folic acid	Sigma-Aldrich	#F8758
myoinositol	Sigma-Aldrich	#I7508
penicillin-streptomycin	Sigma-Aldrich	#P4333
β-mercaptoethanol	Gibco	#31350
collagenase D	Roche	#11088866001
DNase I	Sigma-Aldrich	#D4263
red blood cell lysis buffer	Gibco	#A1049201
cycloheximide	Sigma-Aldrich	CAS No. 66-81-9; Cat. #C4859
Experimental models: Cell lines		
NK-92	ATCC	CRL-2408
Flt3l-producing B16 melanoma (Mach et al.)[58]	Gift from Everts Lab	N/A
Experimental models: Organisms/strains		
Mouse/C57BL/6J	Charles River	Strain code: 632
Mouse/OT I (C57BL/6-Tg(TcraTcrb)1100Mjb/Crl)	Charles River	Strain code: 642
Software and algorithms		
FlowJo version 10.9	BD Biosciences	N/A
Prism 9	GraphPad	N/A

RESOURCE AVAILABILITY

Lead contact

Further information and requests for resources and reagents should be directed to and will befulfilled by the lead contact Linda Sinclair (l.v.sinclair@dundee.ac.uk).

Materials availability

This study did not generate new unique reagents.

Data and code availability

- This study did not generate new datasets. This paper analyzes existing, publicly available data. These data are available at www.ImmPres.co.uk[35].
- This paper does not report new code.
- Any additional information required to reanalyze the data reported in this paper is available from the lead contacts upon request.

EXPERIMENTAL MODEL

Mice

At the Leiden Institute of Chemistry (LIC), C57BL/6J male and female mice were bred under specific pathogen free (SPF) conditions. Animal license number AVD1160020198832. Mice between 6 weeks and 6 months old were culled by cervical dislocation. Animal experiments were approved by the Dutch Central Authority for Scientific Procedures on Animals (CCD) and performed in accordance with European Union Directive 2010/63EU, Recommendation 2007/526/EC and local government regulations.

At the University of Dundee, OT-1 transgenic mice, whose T cell receptor (TCR) was designed to recognize $OVA_{257-264}$ peptide (SIINFEKL), were bred and maintained in the Biological Resource Unit under SPF conditions. Procedures were approved by the University Ethical Review Committee and under the authorisation of the UK Home Office Animals (Scientific Procedures) Act 1986. Male and female mice used were between 8 and 14 weeks old.

In Trinity College Dublin, C57BL/6J mice were bred in house and used between 6 and 12 weeks of age. Mice were housed under 12:12 light cycle in a relative humidity of 45–65% and a temperature between 20°C and 24°C. Mouse experiments were approved by and in compliance with the Irish Health Products Regulatory Authority (Project licence AE19136_P091) and the Animal Research Ethics Committee (AREC) at Trinity College Dublin.

NK92 cell culture

NK92 (ATCC CRL-2408) cells were cultured in RPMI 1640 supplemented with 2 mM glutamine (Gibco), 12.5% horse serum (Sigma), 12.5% fetal calf serum (Biosera), 0.02 mM folic acid (Sigma), 0.2 mM myoinositol (Sigma), 1% penicillin-streptomycin (Gibco) and 0.1 mM β-mercaptoethanol (Gibco). Cells were sub-cultured 1:2 every 2 days and fresh growth medium applied. NK92 cells were gently triturated with a pasteur pipette, counted and seeded in 96-well U-bottomed plates at 0.5 million cells/well before further experimentation.

METHOD DETAILS

T cell isolation and activation

Spleen from C57BL/6J mice were mechanically disrupted using the back-end of a syringe before addition of 50 μL 11x concentrated collagenase D (Roche, #11088866001; end concentration = 1 mg/mL) and DNase I (Sigma, #D4263; end concentration = 2000 U/mL) for 20 min at 37°C, 5% CO_2. After collagenase digestion, the cell suspension was filtered through 70–100 μm sterile filters and centrifuged. Red blood cells were lysed from the splenocyte suspension using red blood cell lysis buffer (Gibco, #A1049201) for 5 min at room temperature. The resultant splenocyte cell suspension was resuspended in RPMI (Sigma, #R5886) supplemented with GlutaMAX (Gibco, #35050061), 10% heat-inactivated fetal calf serum, 50 μM of β-mercaptoethanol (Gibco, #31350), 50 IU/mL penicillin and 50 μg/mL streptomycin: (complete RPMI). To activate primary T cells, single-cell spleen suspensions from C57BL/6J mice were cultured at 5 million cells/mL in complete RPMI with 1 μg/mL anti-CD3 (BioLegend, #100340) and 1 μg/mL anti-CD28 (BioLegend, #102116) for 24h. Naive T cells were seeded from the same spleen suspensions and kept under the same conditions but without anti-CD3/28.

For generation of cytotoxic T cells (CTLs), single-cell suspensions were generated by mashing lymph nodes and/or spleens from OT-1 mice through a 70 μm strainer. Red blood cells in splenocyte suspension were lysed with 5 mls ACK buffer (150 mM NH_4Cl, 10 mM $KHCO_3$ and 110 μM Na_2EDTA in mQ water (pH = 7.8)). Single-cell suspensions were activated using 10 ng/mL $OVA_{257-264}$ peptide (SIINFEKL peptide; in house) at a density of 5 million cells/mL and cultured at 37°C with 5% CO_2 in RPMI 1640 containing glutamine (Invitrogen), supplemented with 10% FBS (Gibco), penicillin/streptomycin (Gibco) and 50 μM β-mercaptoethanol (Sigma)

with cytokines IL-12 (2 ng/mL; Peprotech) and IL-2 (20 ng/mL; Proleukin Novartis). Cells were activated for 36 h, washed out of activation media and then expanded for a further 3–4 days in media supplemented with 20 ng/mL IL-2.

In vivo DC expansion

Flt3l-producing B16 melanoma cells[58] were used to expand the DC population *in vivo* as previously described.[36] Briefly, 2.5 million melanoma cells in 100 μL PBS were injected subcutaneously into the right flank of the mouse. After 10 days of tumor growth, the mouse was culled, and the spleens processed as described above.

Bioorthogonal amino acid uptake by flow cytometry

Maintain the temperature of the cells and buffers between 37°C and room temperature, except for those used for uptake at 4°C (cold controls).

Cells were washed using equal parts HBSS (Gibco, #24020) and RPMI (HBSS:RPMI+GlutaMAX), and centrifuged again. After removal of supernatant, the cell pellet was resuspend in HBSS:RPMI+GlutaMAX and counted. Cells were pre-stained with LIVE/DEAD Fixable Aqua Dead Cell Stain (Thermo, #L34957) in the dark for 20 min at room temperature. 500′000 cells in HBSS were seeded into v-bottom 96-well plate wells.

In parallel, 80 μL of an HBSS solution with twice the concentration of bioorthogonal amino acid as indicated in the graphs (+/− control competing amino acids as indicated) were added to 96-well plate wells and either warmed in a cell incubator (37°C) or chilled on ice (4°C = cold controls) for 15 min to equilibrate the temperature. 50 μL of this click AA 2x concentrate was then added to 50 μL of cells and plates were returned to the incubator or ice to incubate for the designated amount of time. Afterward, 100 μL of 2% paraformaldehyde solution (Polysciences, #18814-20; methanol free; final concentration = 1%) in HBSS was added to each well and the plates were incubated in the dark for 30 min at room temperature. Plates were centrifuged, supernatant was removed, and cell pellets were resuspended in phosphate-buffered saline (PBS). Cells were kept in this PBS and at 4°C for later click chemistry and flow cytometry antibody staining.

For determining sodium dependence of amino acid uptake, buffers were prepared with 2 mM KCl (Sigma, # 60128), 1 mM $CaCl_2$ (Merck, #1.02389), 1 mM $MgCl_2$ (Ambion, #AM9530) and 10 mM (HEPES; inhouse; pH = 7.5) in MQ water and with either 100 mM NaCl (TJ Baker, #277) for the sodium-containing buffer or 100 mM tetramethylammonium chloride (TMACl) for the sodium-free buffer.

Azidohomoalanine (AHA) and homopropargylglycine (HPG) were synthesized as described previously.[44,59] Azidoglutamine was bought From Chiralix (#CX57717).

Click chemistry

Cells were permeabilized for 20 min at room temperature using 0.01% saponin (Sigma, #47036) in PBS after the plate was centrifuged and supernatant was removed. Near the end of permeabilization the click-mixture was prepared.

In a sequential order sodium ascorbate (NaAsc), tris-hydroxypropyltriazolylmethylamine (THPTA), aminoguanidine, PBS and bioorthogonal fluorophore were added to copper sulfate ($CuSO_4$). This together is called the click-mixture, 'click-mix' and is used for incubating the cells. Upon combination of light blue $CuSO_4$ and the light yellow NaAsc, the solution turns dark brown/black. Upon subsequent addition of the THPTA, the solution turns pale yellow/colourless. We used 1 part of $CuSO_4$ (Sigma, #209198; stock 100 mM in Milli-Q [MQ] water, final concentration 1 mM) together with 1 part of NaAsc (Sigma, #A7631; stock 1 M in MQ, final concentration 10 mM), 1 part of THPTA (stock 100 mM in MQ, final concentration 1 mM), 1 part of aminoguanidine (Cayman Chemicals, #81530; stock 1 M in MQ, final concentration 10 mM), 96 parts of PBS and 0.25 part of bioorthogonal fluorophore (AZDye 488 alkyne, AZDye 488 azide, AZDye 647 alkyne, AZDye 647 azide; all Click Chemistry Tools, #1277, #1275, #1301 and #1299 respectively; 2 mM in DMSO, final concentration 5 μM).

After permeabilization, the plate was centrifuged, supernatant was removed, and cell pellets were resuspended in 30 μL of click-mix and incubated in the dark for 1 h at room temperature. The plate was centrifuged, copper-containing click-mix supernatant was discarded in accordance with the institute recommendations for aqueous copper disposal, cell pellets were resuspended in 200 μL of PBS supplemented with 0.5% bovine serum albumin [BSA; Sigma, #A9467] and 2 mM ethylenediaminetetraacetic acid [EDTA; from inhouse stock of 0.5 M at pH = 8.0] (FACs buffer) and incubated for 30 min in the dark. The plate was centrifuged, any residual copper-containing supernatant was discarded in the same manner as before and cells were washed one more time with FACS buffer before antibody staining and normal washes and supernatant removal and acquisition on the flow cytometer. THPTA was synthesized as described earlier.[41]

Measuring protein synthesis

O-propargyl-puromycin (OPP, Thermofisher, Cat# C10459) was used to measure protein synthesis in NK92 and splenocytes. Incorporation was measured using the Cu-catalyzed click reaction as above to attach and azido-fluoorphore, fluorescence intensity reflects of the level of protein synthesis. OPP (25 μM) was incubated in complete medium for 20 min, then cells were fixed using 2% PFA for 15 min, and permeabilized with 1% BSA/0.01% Saponin for 20 min. Cu-catalysed click reaction was performed for 1 h at room temperature using an azide-AF594 as the probe. As a control to confirm OPP was measuring protein synthesis, cells were pre-treated with cycloheximide (CHX, 100 μg/mL), a potent inhibitor of protein synthesis, for 10 min prior to incubation with OPP.

Double click assay using OPP and AHA

To simultaneously measure protein synthesis and SLC1A5-mediated amino acid uptake a sequential double click reaction was performed. Cells were harvested as previously described and surface stained, then resuspended in medium containing OPP (25 μM) for 20 min at 37°C. Cells were washed with PBS and resuspended in HBSS for 10 min at either 37°C or 4°C. AHA in HBSS was added to the cells (final AHA concentration 100μM, HBSS:media ratio was 1:3) and incubated at 37°C or 4°C for 2 min. Cells were fixed by adding 2% PFA (final concentration 1% PFA) for 15 min. Cells were washed with PBS and resuspended in permeabilization buffer containing 1% BSA and 0.01% Saponin for 20 min. Click reactions were then performed for both OPP and AHA using respective azide or alkyne probes, azide-AF594 and alkyne. Each click reaction was performed for 1 h at room temperature with 2X PBS washes in between reactions. Finally the cells were washed ×3 with PBS before analysis.

Flow cytometry

Antibody staining was done in the dark for 30 min at 4°C in 30 μL of FACS buffer with antibodies and anti-CD16/32 (TruStain FcX PLUS; BioLegend, #156604; 1:100). Acquisition was done on a BD FACSCanto II or BD LSRFortessa (both BD Biosciences). Analysis, including dimensionality reduction by t-distributed stochastic neighbor embedding (tSNE), was done using FlowJo (TreeStar, version 10).

Flow cytometry antibodies

Spleen T cell staining panel

B220 - PerCP-Cyanine5.5 (BioLegend, #103236; 1:400), CD4 – PE-Cyanine7 (BioLegend, #100422; 1:400), I-A/I-E (MHC class II) – APC (BioLegend, #107613; 1:4000) and CD8a – APC-Cyanine7 (BioLegend, #100714; 1:400) was combined with AZDye 488 alkyne/azide. When AZDye 647 alkyne/azide was used, MHCII – APC was replaced by MHCII – FITC (eBioscience, #11-5321-82; 1:2000). In this panel, LIVE/DEAD Fixable Aqua was stained before the other markers using a 1:400 dilution.

Spleen cDC staining panel

CD3 – APC (BioLegend, #100312; 1:200), CD19 – PE-Cyanine7 (BD Horizon, #552854; 1:200), F4/80 – AF700 (Bio-Rad, #MCA497A700; 1:200), I-A/I-E (MHCII)-APC-eFluor 780 (eBioscience, #47532182; 1:400), CD11c – Brilliant Violet 421 (BD Horizon, #562782; 1:200), CD8a - PerCP-Cyanine5.5 (BD, #551162; 1:200), CD11b – Brilliant Violet 605 (BioLegend, #101257; 1:200), XCR1 – Brilliant Violet 785 (BioLegend, #148225; 1:200) and CD317 – Brilliant Violet 650 (BioLegend, #127019; 1:200) combined with AZDye 488 alkyne/azide.

Thymocyte staining panel

CD24 – Brilliant Violet 421 (BioLegend, #101825; 1:400), Lineage cocktail – PE (Nk-1.1 – PE [BD Biosciences, #557391; 1:100], Gr-1 – PE [eBioscience, #12-5931-82; 1:400], CD19 – PE [eBioscience, #12-0191-83; 1:100], CD11b – PE [eBioscience, #12-0112-81; 1:800]), CD25 – PerCP-Cyanine5.5 (BD Biosciencs, #561112; 1:100), CD44 – PE-Cyanine7 (eBiosciences, #25-0441-81; 1:600), CD4 – APC (eBiosciences, #17-0042-83; 1:200) and CD8a – APC-Cyanine7 (BioLegend, #100714; 1:400) combined with AZDye 488 alkyne/azide. In this panel, LIVE/DEAD Fixable Aqua was stained before the other markers using a 1:400 dilution.

OPP staining panel

CD3 – FITC (eBiosciences, #464882), CD4-PE-Cyanine7 (BD Pharmingen, #552775), CD8-PerCP-Cyanine5.5 (BD Pharmingen, #551162), MHCII-APC-eFluor 780 (eBiosciences), CD11c – Brilliant Violet 421 (BD Horizon, #562782), CD11b-Brillant Violet 510 (BD Horizon, #562950), CD19-Brilliant Violet 650 (BD Horizon, #563235) and XCR1-Brilliant Violet 785 (BioLegend, #148225) combined with AZDye 594 azide (Click Chemistry Tools, #1295) and AZDye 488 alkyne for OPP and AHA detection respectively. In this panel, Zombie Yellow Fixable Viability Kit (BioLegend, #423103) was stained before the other markers according to the manufacturer's recommendations.

Confocal microscopy

Confocal microscopy was performed using a Leica SP8 scanning confocal microscope. After 10 min of FC block (BD Biosciences, 1:100), splenocytes were stained for 30 min at room temperature with anti-mouse XCR1 conjugated to AF647 (BioLegend) to identify $XCR1^+$ cells. Splenocytes were then washed with PBS, resuspended in HBSS for uptake assays and allowed to reach temperature either in a 37°C incubator or on ice. The uptake assay was performed as described above. After HPG uptake, cells were immediately fixed with 1% PFA for 30 min at room temperature. Splenocytes were permeabilised with PBS containing 1% BSA and 0.01% saponin. The click reaction was performed as described above using azido-AF488 in the click-mix. Cells were washed 4 times with PBS and resuspended in PBS containing 1% BSA and DAPI (1 μg/mL; Sigma) as a nuclear stain. Splenocytes were stained for 45 min with DAPI before washing. Finally, cells were resuspended in a mounting medium (Mowiol, Sigma) and pipetted directly onto high-resolution microscope slides. The mounting medium was allowed to set overnight at room temperature in the dark before imaging. Quantification of mean pixel intensity was performed on IMARIS imaging software by generating a pixel mask for the green fluorescence channel after setting a suitable threshold to negate background fluorescence.

Radiolabeled ^{3}H-glutamine uptake

Briefly, L-[3,4^{3}H(N)]-glutamine (^{3}H-glutamine; PerkinElmer, #NET551001MC) uptake was carried out using 1 million cells resuspended in 0.4 mL HBSS (Thermo, #14025092) containing ^{3}H-glutamine (0.5 μCi/mL) and layered over 0.5 mL of 1:1 silicone oil:dibutyl phthalate (Sigma-Aldrich, #175633 and #524980 respectively). Uptake time was 3 min, after which cells were pelleted below the oil via centrifugation, stopping uptake. The aqueous supernatant solution, followed by the silicone oil/dibutyl phthalate mixture, was aspirated and the cell pellet resuspended in 200 μL of 1 M NaOH. β-radioactivity was measured by liquid scintillation counting in a Beckman LS 6500 Multi-Purpose Scintillation Counter (scintillant Optiphase HiSafe 3; PerkinElmer, #1200.437). L-Alanine (Sigma, #A7627), L-Glutamine (Sigma, #G8540), 2-Amino-2-norbornanecarboxylic acid (BCH; Sigma, #A7902), α-(Methylamino)isobutyric acid (MeAIB; Sigma, #M2383), AHA or HPG were used at titrating concentrations or 5 mM to inhibit radiolabeled ligand uptake as indicated in the graphs.

In vivo administration of HPG

In vivo administration of HPG was performed using OT-I transgenic mice. Briefly, 25μg of ODN1826 (Invivogen, #tlrl-1826) and 25μg of OVA protein (Invivogen) were resuspended in 25μL of PBS which was administered subcutaneously into the ankle by hock injection.[60] After 24h, 25μL of 10 mg/ml HPG was administered subcutaneously into the ankle of the same mice. After 40 min, mice were culled and popliteal and cervical lymph nodes were harvested. Lymph nodes were mechanically digested into a single cell suspension by passing through a 70μm cell filter before surface phenotype staining, fixing and click reaction as described above.

QUANTIFICATION AND STATISTICAL ANALYSIS

Statistical tests were performed using Graphpad software, Prism version 9. Data was analyzed using students t-test, one way ANOVA with a Dunnet's, Tukey or Sidak's post-test or two-way ANOVA with a Dunnet's post-test as indicated.